

Astronomy & Astrophysics manuscript no.
 (will be inserted by hand later)

Hard X-ray properties of blazars

D. Donato¹, G. Ghisellini¹, G. Tagliaferri¹, and G. Fossati²

¹ Osservatorio Astronomico di Brera, Via Bianchi 46, I-23807 Merate, Italy

² Center for Astrophysics and Space Sciences, University of California at San Diego, 9500 Gilman Drive, La Jolla, CA 92093-0424, USA

Received date / accepted date

Abstract. We have considered all blazars observed in the X-ray band and for which the slope of the X-ray spectrum is available. We have collected 421 spectra of 268 blazars, including 12 archival unpublished ASCA spectra of 7 blazars whose analysis is presented here. The X-ray spectra of blazars show trends as a function of their power, confirming that the blazar overall energy distribution can be parameterized on the basis of one parameter only, i.e. the bolometric luminosity. This is confirmed by the relatively new hard (2–10 keV) X-ray data. Our results confirm the idea that in low power objects the X-ray emission mechanism is the synchrotron process, dominating both the soft and the hard X-ray emissions. Low energy peaked BL Lac objects are intermediate, often showing harder spectra in the hard X-ray band, suggesting that the synchrotron process dominates in the soft band, with the inverse Compton process dominating at high energies. The most powerful objects have X-ray spectra that are flat both in the soft and in the hard band, consistent with a dominating inverse Compton component.

Key words. BL Lacertae objects: general – X-rays: galaxies

1. Introduction

Thanks to γ -ray observations of EGRET, on board CGRO, we now know the overall spectral energy distribution (SED) of blazars. They are characterized, in $\nu - \nu F(\nu)$ plots, by two broad peaks. It is believed that the first, located in the IR–soft X-ray band, is due to synchrotron emission, while the second is due to the inverse Compton process by the same electrons producing the synchrotron part of the spectrum (Maraschi, Ghisellini & Celotti 1992; Sikora, Begelman & Rees 1994; but see Mannheim 1993 for a different interpretation). The 0.1–10 keV emission of blazars is therefore located in the minimum between the two peaks, where both processes (synchrotron and inverse Compton) can contribute. Observations in this band are therefore useful to characterize the relative importance of both processes. This can constrain models, allowing a better determination of the location of both peaks. Usually, a steep power law energy distribution in the X-ray band (with a spectral energy index $\alpha > 1$, with $F \propto \nu^{-\alpha}$) is due to the tail of the synchrotron spectrum, while $\alpha < 1$ flags the dominance of the inverse Compton spectrum. There are exceptions to this rule, such as HBL (High energy peaked BL Lacs) in a flaring state, which show a synchrotron spectrum peaking above 10 keV. One dramatic example of this behavior is Mkn 501, whose synchrotron

peak energy, usually located below/at $\simeq 1$ keV, shifted to 100 keV or more during its flare in April 1997 (Pian et al. 1998). In these cases the X-ray spectrum, usually steep during quiescence, becomes much flatter during flares.

Fossati et al. (1998) (F98 hereafter) have shown that blazars form a sequence, with their SED changing in a continuous way as their bolometric power changes: low luminosity objects (HBL) have the synchrotron peak in the UV–soft X-ray band, and the inverse Compton peak between the GeV and the TeV band. The two components have approximately the same power. As the bolometric luminosity increases, both peaks shift to lower frequencies, and the Compton peak becomes increasingly dominant. This trend offers the opportunity to unify in a single scheme the many flavors of existing blazars, and calls for a physical explanation (see e.g. Ghisellini et al., 1998).

To check the reliability of this trend we have collected data for all blazars having available spectral information in the X-ray band. For the soft band [0.1–2 keV] most of the results come from *ROSAT*, while for the 2–10 keV band the results are gathered from the EXOSAT, ASCA and *BeppoSAX* satellites.

Besides the data already published, we searched for unpublished data in the ASCA public archive, finding 12 observations of 7 sources. Results of the analysis of these data are presented here. We then add these sources to our sample.

The entire sample forms the largest database in the X-ray range: 421 spectra of 268 blazars. The X-ray data have been complemented by additional information regarding the redshift (when available), the radio flux at 5 GHz and the optical flux (in the V band).

The paper is organized as follows; section 2 is devoted to the analysis of the 12 ASCA spectra, while in Section 3 we present the entire set of data. In Section 4 we compare the results in the soft and the hard X-ray bands and check for correlations with other spectral parameters, such as the broad band spectral indices connecting the radio with the optical fluxes, the optical with the X-ray fluxes, and the radio with the X-ray fluxes. In Section 5 we discuss our findings in the framework of the scenario proposed by Fossati et al. (1998), suggesting an improvement connected to a possible physical difference between low and high power sources.

2. Analysis of ASCA data

We searched the ASCA public archive at HEASARC, finding 12 observations of 7 blazars that have not been analyzed and published before: 0405–123 and PKS 0420–014 (classified as Flat Spectrum Radio Quasars, FSRQs); B2 1308+326 and 1807+698 (classified as Low Peaked BL Lac objects, LBLs); 1ES 1028+511, 1553+511 and 1ES 2344+514 (classified as High Peaked BL Lac objects, HBLs).

1ES 1028+511 and 1ES 2344+514 have 3 separate observations each, while B2 1308+326 was observed twice. The search for unpublished observations is updated to November 1999. During the preparation of this work the "Tartarus" data base became available¹, presenting results of an automatic spectral and temporal analysis for the AGNs observed by ASCA.

2.1. Data Reduction and Spectral Analysis

We extracted the spectra of all sources from the files produced by the Revision–2 data release and included data transmitted in all 3 modes (High, Medium and Low) to increase the signal/noise ratio. The event files are obtained from all four instruments on board ASCA: the Solid-State Imaging Spectrometers (SIS0 and SIS1) and the Gas Imaging Spectrometers (GIS2 and GIS3). For the SIS we used the event files converted into BRIGHT mode. For a description of the ASCA observatory see e.g. Tanaka et al. (1994).

To screen the SIS and GIS data we follow the criteria given in the *ABC ASCA reduction guide*, rejecting the data taken during the passage of the South Atlantic Anomaly, or with geomagnetic cutoff rigidity lower than 8 GeV/c, or with angles between the targets and the day/night terminator smaller than 20° or for Elevation angles smaller than 5° .

The source spectra were extracted from circular regions centered on the sources, with radii of 6 arcmin for the GIS and 4 arcmin for the SIS0, while for the SIS1 the source is normally nearer to the detector border and we had to use a smaller radius of ~ 3.3 arcmin. For the GIS we extracted the background in circular regions with the same dimensions used for the sources but centered on a symmetric point with respect to the optical axis, where the contribution of the source to the counts was negligible. For the SIS, instead, the background was extracted from blank field files because the sources occupied a large area of the detector. On these blank fields we chose circular regions with the same radii and positions used for the sources.

For the GIS spectra we used the 1994 May response matrices, while for the SIS spectra we generated the matrices with the SISRMG program of the FTOOLS V3.6 package. The ARF files for both SIS and GIS were derived with the ASCAARF V2.62 program. The GIS and SIS data were fitted in the channel ranges 69–1020 and 15–510, corresponding to the energy ranges 0.7–10 and 0.4–10 keV, respectively. The spectra were rebinned in order to have at least 25 counts in each new bin.

The ASCA spectra were fitted using XSPEC V10 with four models: single or broken power law with free or fixed (Galactic) absorption. The cross section for photoelectric absorption is calculated following Morrison & McCammon (1983), while the Galactic column density in the direction of the sources was estimated from the 21cm radio maps of neutral hydrogen (Brinkmann & Siebert, 1994; Danly et al., 1992; Dickey & Lockman, 1990; Elvis et al., 1989; Lamer, Brunner & Staubert, 1996; Lockman & Savage 1995; Murphy et al. 1996). The data were fitted simultaneously from all the instruments with the same model. However, the normalizations were left as independent parameters for each data set to account for the cross-calibration uncertainties between the four detectors, estimated to be of the order of 6%. The differences found between the various normalizations were always consistent with these uncertainties.

2.2. Results of the fits

The results of the 12 spectral fits of the 7 blazars observed by ASCA are reported in Table 1. The uncertainties for the spectral parameters are at the 90% confidence errors for two parameters of interest ($\Delta\chi^2 = 4.6$). The unabsorbed integrated 2–10 keV and monochromatic 1 keV fluxes are obtained using only the SIS0 data. As the observations presented in this paper were all taken after 1994, they are most likely affected by the so-called "excess N_H " problem. This is due to a degradation of the SIS efficiency below 1 keV which can give incorrect results for the column density and/or other parameters. As suggested in the ASCA Web site, to avoid the calibration uncertainties we considered only the SIS data above 1 keV in the SIS+GIS combined fit. Of the four models considered, according to

¹ at <http://tartarus.gsfc.nasa.gov/>

Source	Obs. date ^a	N_{H} 10^{21} cm^{-2}	Γ	χ^2/dof	$F_{[2-10]}^b$	$F_{1\text{keV}}$ μJy
0405–123	09/08/1998	$0.72^{+0.51}_{-0.63}$	$1.76^{+0.09}_{-0.10}$	1.0/160	5.2	0.9
0420–014	31/08/1997	$0.90^{+1.04}_{-0.81}$	$1.86^{+0.19}_{-0.18}$	0.8/73	1.4	0.3
1028+511	28/04/1995	$1.01^{+0.23}_{-0.21}$	$2.53^{+0.06}_{-0.05}$	1.0/287	6.2	3.4
	29/04/1995	$1.33^{+0.18}_{-0.17}$	$2.59^{+0.05}_{-0.05}$	0.9/310	7.4	4.5
	08/05/1995	$1.12^{+0.12}_{-0.12}$	$2.49^{+0.04}_{-0.04}$	0.9/201	7.8	4.1
1308+326	10/06/1996	$1.97^{+2.96}_{-1.97}$	$1.99^{+0.47}_{-0.36}$	1.5/29	0.5	0.1
	11/06/1996	$0.97^{+1.01}_{-0.97}$	$1.74^{+0.32}_{-0.23}$	1.4/78	0.6	0.1
1553+113	16/08/1995	$1.30^{+0.62}_{-0.61}$	$2.47^{+0.19}_{-0.18}$	1.3/294	29.4	14.9
1807+698	05/11/1996	$0.50^{+0.28}_{-0.27}$	$1.75^{+0.07}_{-0.06}$	1.0/122	3.1	0.5
2344+514	10/01/1997	$2.71^{+0.17}_{-0.17}$	$2.13^{+0.03}_{-0.03}$	1.1/216	17.2	5.3
	23/01/1997	$2.91^{+0.34}_{-0.33}$	$2.39^{+0.08}_{-0.06}$	0.9/72	10.4	5.2
	10/12/1997	$2.93^{+0.37}_{-0.35}$	$2.31^{+0.07}_{-0.07}$	1.2/202	10.4	4.2

Table 1. Best fits of the 12 observations. a) day/month/year; b) $10^{-12} \text{ erg cm}^{-2} \text{s}^{-1}$

the F-test, the one that better represents the data in all twelve cases is the single power law with free N_{H} . In some cases (detailed below) we obtain a value for the absorbing column greater (by a factor 3–10) than the Galactic value. Note that the results obtained by the automatic analysis presented in the “Tartarus” database are in excellent agreement with ours (not surprisingly, since the same model is adopted). What is somewhat surprising is that the broken power law model (either with free or fixed N_{H}) did not significantly improve the fits. This may be indicative of true extra-absorption or a spectral behavior more complex than those here examined (one possibility being a gradual but continuous steepening of the spectrum).

In the following we will compare the spectral properties of blazars in the soft and hard X-ray bands considering only the single power law model. To this end the results of this model allow a more uniform comparison.

The results of spectral fit for the 7 sources are discussed below, grouped in the three subclasses (FSRQ, LBL and HBL).

2.2.1. FSRQ

For 0405–123, the best fit gives a flat photon spectral index $\Gamma = 1.76 \pm 0.1$, indicating the dominance of the inverse Compton component. The derived N_{H} value is consistent with the Galactic value, $N_{\text{H}}^{Gal} = 0.37 \times 10^{21} \text{ cm}^{-2}$ (Danly et al. 1992).

Similar results are obtained for PKS 0420–014, with a photon spectral index $\Gamma = 1.86 \pm 0.19$. Also in this case the N_{H} value is consistent with the Galactic one ($N_{\text{H}}^{Gal} = 0.94 \times 10^{21} \text{ cm}^{-2}$, Elvis et al. 1989).

2.2.2. LBL

For B2 1308+326 there are two observations on two consecutive days. The spectra are quite noisy and also the reduced χ^2_r are not very good. In both cases the best fits are obtained with a spectral index $\Gamma \simeq 1.75\text{--}2.0$. Due to the large error bars (see Table 2.1), the derived absorp-

tion column density can be consistent with the Galactic one ($N_{\text{H}}^{Gal} = 0.11 \times 10^{21} \text{ cm}^{-2}$, Lockman & Savage 1995).

For 1807+698 we obtained $\Gamma = 1.75 \pm 0.07$ and a value of N_{H} consistent with the Galactic one ($N_{\text{H}}^{Gal} = 0.44 \times 10^{21} \text{ cm}^{-2}$, Murphy et al. 1996).

2.2.3. HBL

1ES 1028+511 has been observed three times over a time span of two weeks. The source did not significantly vary in flux nor in shape ($\Delta\Gamma \simeq 0.12$). In all cases the best fits are obtained for a value of N_{H} a factor 10 larger than the Galactic one ($N_{\text{H}}^{Gal} = 0.12 \times 10^{21} \text{ cm}^{-2}$; Lamer, Brunner & Staubert, 1996).

For 1553+113 the best fit is obtained with a value of $N_{\text{H}} \sim 3$ times larger than the Galactic one ($N_{\text{H}}^{Gal} = 0.37 \times 10^{21} \text{ cm}^{-2}$; Brinkmann & Siebert, 1994).

The source 1ES 2344+514 has been observed three times, twice in Jan 1997 and one in Dec 1997. Both the fluxes and the spectral indices show some variability. The best fit value for the N_{H} is about 1.5 times the Galactic value ($N_{\text{H}}^{Gal} = 1.67 \times 10^{21} \text{ cm}^{-2}$ Dickey & Lockman, 1990).

3. The catalogue

3.1. Starting samples

Our purpose is to have the most complete ensemble of spectral information (fluxes and spectral indices) in the X-ray band, from 0.1 to 10 keV, of all known blazars. We therefore considered all blazars detected in the X-ray band, for which also a measure of the X-ray spectral index is available. We collected the data obtained by five X-ray satellites: *Einstein*, EXOSAT, ROSAT, ASCA and *BeppoSAX* (see Table 2).

The first step was to recognize if a source belongs to the blazar class, and to which subclass (i.e. if a source is a FSRQ or an HBL or an LBL). We used several published lists of blazars and other publications describing single recognized sources. We considered the Slew Survey Sample (Elvis et al. 1992, Perlman et al. 1996), the 2 Jy

sample of Wall & Peacock (1985), and the 1 Jy BL Lac sample (Stickel et al. 1991). In addition, we used the lists taken from the works of Bade et al. (1994), Bade et al. (1998), Brinkmann et al. (1994), Brinkmann et al. (1997), Cappi et al. (1997), Comastri et al. (1997), Ghisellini et al. (1993), Lamer et al. (1996), Laurent-Muehleisen et al. (1999), Sambruna et al. (1997), Wolter et al. (1998) and Worrall et al. (1990). We also checked the NASA Extragalactic Database (NED) for other objects classified as BL Lacs/blazars, or that could be classified as such.

The total number of considered blazars is 268. Of these, 227 have been observed by *ROSAT* and 88 have spectral information in the 2–10 keV band [of these latter sources, 77 have both soft (*ROSAT*) and hard X-ray data]. The details about the breakdown of source among HBL/LBL/FSRQ, and of the data among different X-ray telescopes is reported in Table 2. The data obtained with *Einstein* have large errors associated and for almost all sources better *ROSAT* data were available. For these reasons, the Einstein data are not used to derive any of the results (or figures) of this paper.

Some sources have been observed many times either by the same and/or by different satellites. For these sources, we chose the observation with the best χ^2_r in the analysis².

For the most “famous” sources, like 3C 273, Mkn 421, Mkn 501, PKS 2155–304, we do not include the results of all the observations made by all satellites, but we have only listed few representative data (those with the best χ^2_r) for each of these sources (typically, one spectral datum for each observing satellite).

Of course, the resulting catalogue is not a complete sample. Nevertheless, it is the largest database of its kind, and we think it is representative of the entire blazar class. The large number of sources in each sub-category of blazars guarantees a meaningful comparison between their X-ray properties, and their relation with the fluxes in other bands.

3.2. Format of the catalogue

Data are presented in Table 7 with the following format. For each source, Table 7 gives the IAU name, the redshift, the fluxes in the radio band (5 GHz), optical (V band) and X-ray (1 keV) and the X-ray photon spectral index. In the last columns of Table 7 we also indicate to which subclass the blazar belongs to (1 for HBL, 2 for LBL and 3 for FSRQs) and the observing satellite (RO=*ROSAT*; AS=*ASCA*; EI=*Einstein*; EX=*EXOSAT*; SA=*BeppeSAX*).

² We have verified that this choice does not introduce a bias towards particularly faint states of the sources (for which lower statistics could yield larger error bars and better χ^2) nor towards particularly high states (for which a better statistics could yield lower values of the reduced χ^2 due to the increased number of degrees of freedom).

	N°oss.	HBL	LBL	FSRQ
ASCA	52	14	9	24
EXOSAT	33	16	7	10
<i>BeppeSAX</i>	47	29	9	8
<i>ROSAT</i>	227	129	54	44
<i>EINSTEIN</i>	62	7	23	32
TOTAL	421	136	63	69

Table 2. Number of observations obtained from various satellites and number of observed blazars (divided into different subclasses). For the total number of sources we have excluded multiple observations by different satellites of the same source.

For the radio fluxes we calculated the averaged value when there was more than one observation; the optical fluxes reported in the NED database are calculated using the indicated magnitude dereddened with the galactic extinction A_B as reported by the NED database. When in the literature we found only the 0.1–2.4 keV and/or the 2–10 keV integrated fluxes, we derived the monochromatic ones at 1 keV using the corresponding X-ray spectral index. All fluxes presented in Table 7 are not K-corrected.

To compute the luminosities, we used $H_0=50 \text{ km s}^{-1} \text{ Mpc}^{-1}$ and $q_0=0.5$, and for the K-correction we assumed a radio spectral index $\alpha = 0$ for all sources; an optical spectral index $\alpha = 0.5$ for HBL and $\alpha = 1$ for the rest of the sources; for the X-ray data we used the listed X-ray spectral index. Also the broad band spectral indices have been K-corrected.

The K-correction for sources with unknown redshift was computed using the average redshift appropriate for each sub-class (i.e. $\langle z \rangle_{HBL} = 0.249$, $\langle z \rangle_{LBL} = 0.457$ and $\langle z \rangle_{FSRQ} = 1.265$).

4. Results

Theoretical models that explain the nature of the observed behaviors of blazars predict a continuity between the various subclasses. To check if this is true for the objects belonging to our catalogue, we computed the distributions of redshifts, X-ray and broad band spectral indices and luminosities.

Moreover, another goal of this work is to compare the blazar characteristics observed in the soft and in the hard X-ray band. We divided our sources into two groups, one with the data obtained with *ROSAT* (0.1–2.4 keV) and another one with the data obtained with EXOSAT, ASCA, and *BeppeSAX* (2–10 keV). As anticipated (see Table 2) the first group of sources contains 227 objects, while the second one contains 88 sources (38 HBL, 19 LBL and 31 FSRQ). In addition, since the two sources 2344+514 and 1652+398 are very variable and we have data both for a quiescent and a flaring state, in the latter group we put the data of two observations (one for the high and one for the low state) for each of them.

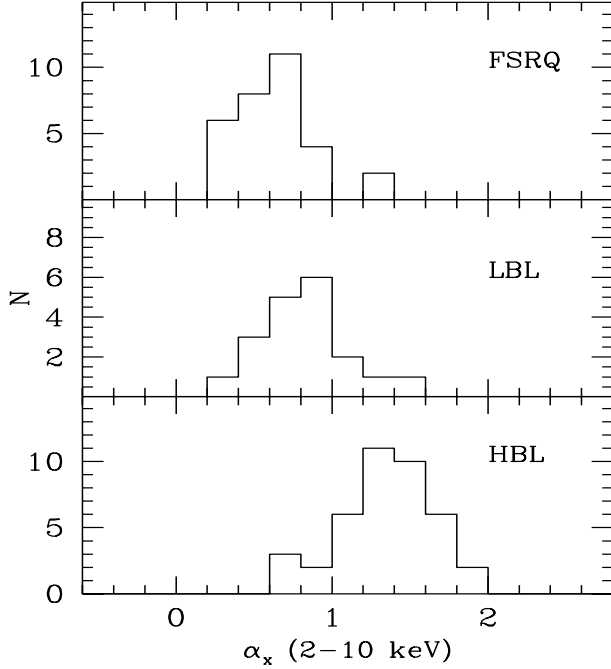


Fig. 1. Distribution of the energy spectral index α_x in the 2–10 keV hard X-ray energy band. Note the difference between the HBL and the other two subclasses of blazars. The KS test gives a probability $P = 8 \times 10^{-6}$ that the HBL and the LBL values are drawn from the same distribution ($P = 2 \times 10^{-12}$ for HBL–FSRQ and $P = 0.03$ for LBL–FSRQ).

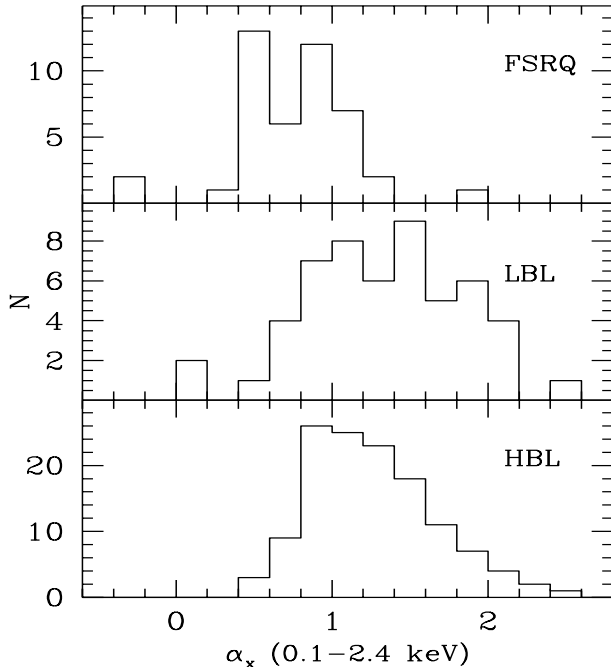


Fig. 2. Distribution of the energy spectral index α_x in the 0.1–2.4 keV soft X-ray energy band. In this case LBL are more similar to HBL than to FSRQ. KS test results: $P = 0.20$ for HBL–LBL; 10^{-8} for HBL–FSRQ; 5×10^{-8} for LBL–FSRQ.

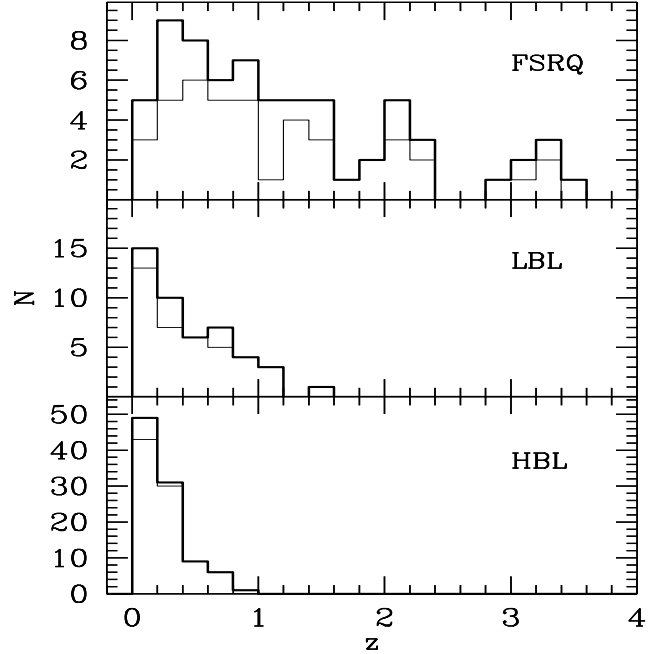


Fig. 3. Redshift distribution for the three subclasses. Thick solid lines refer to the entire sample, while thin solid lines refer to sources with only *ROSAT* data. KS test results (for the entire sample): $P = 2 \times 10^{-3}$ for HBL–LBL; 9×10^{-17} for HBL–FSRQ; 5×10^{-5} for LBL–FSRQ.

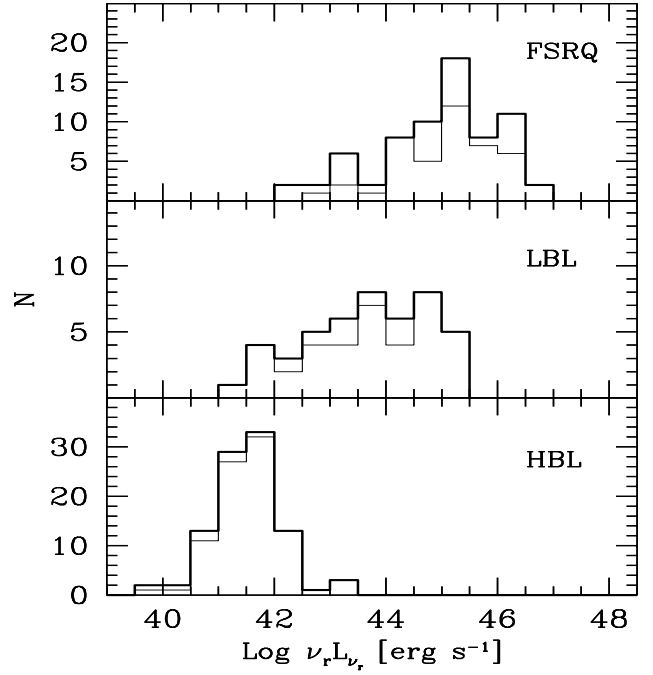


Fig. 4. Distribution of the radio luminosity for the three subclasses. Thick solid lines refer to the entire sample, while thin solid lines refer to sources with only *ROSAT* data. KS test results (for the entire sample): 7×10^{-19} for HBL–LBL; 7×10^{-33} for HBL–FSRQ; 10^{-6} for LBL–FSRQ.

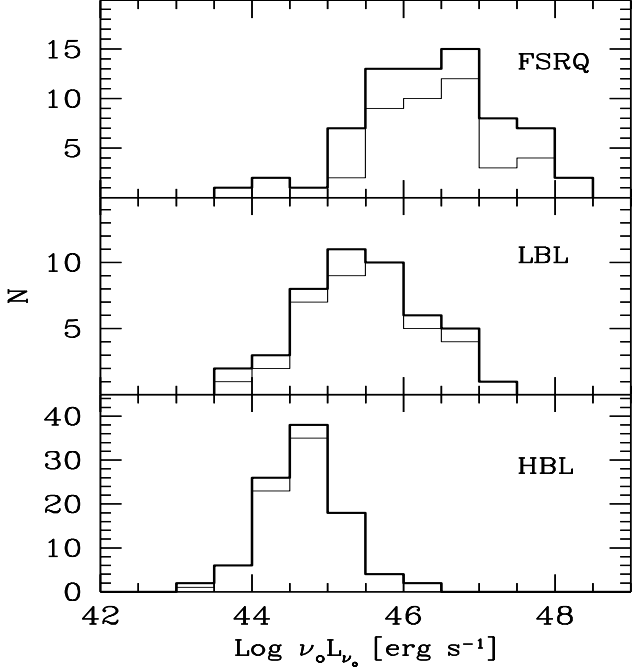


Fig. 5. Distribution of the optical luminosity for the three subclasses. Thick solid lines refer to the entire sample, while thin solid lines refer to sources with only *ROSAT* data. KS test results (for the entire sample): $P = 2 \times 10^{-7}$ for HBL-LBL; 10^{-22} for HBL-FSRQ; 3×10^{-5} for LBL-FSRQ.

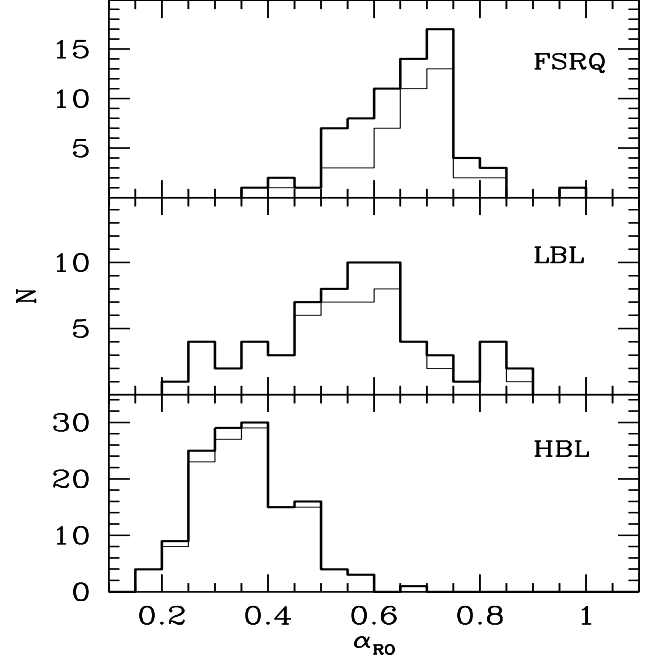


Fig. 7. Distribution of the broad band radio-optical spectral index for the three subclasses. Fluxes have been K-corrected as explained in the text. Thick solid lines refer to the entire sample, while thin solid lines refer to sources with only *ROSAT* data. KS test results (for the entire sample): $P = 4 \times 10^{-18}$ for HBL-LBL; 2×10^{-35} for HBL-FSRQ; 4×10^{-4} for LBL-FSRQ.

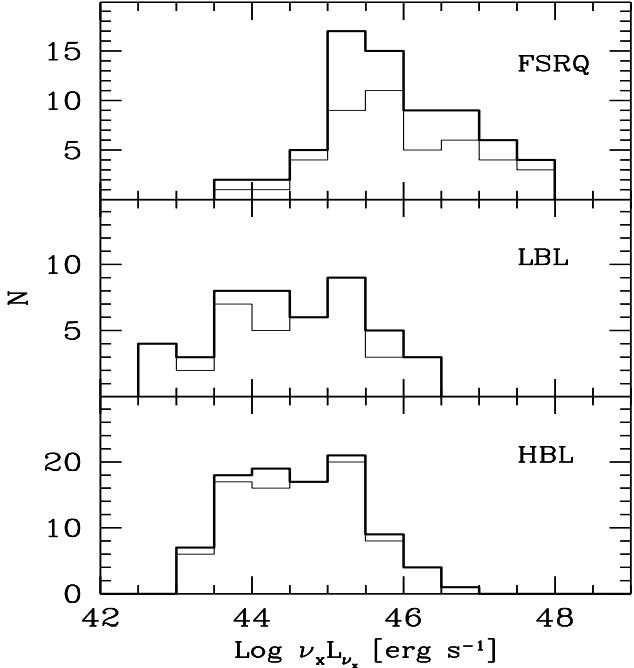


Fig. 6. Distribution of the X-ray luminosity for the three subclasses. Thick solid lines refer to the entire sample, while thin solid lines refer to sources with only *ROSAT* data. KS test results (for the entire sample): $P = 0.6$ for HBL-LBL; 3×10^{-13} for HBL-FSRQ; 2×10^{-8} for LBL-FSRQ.

	HBL	LBL	FSRQ
α_x [2–10 keV]	1.34 ± 0.05	0.84 ± 0.07	0.65 ± 0.04
α_x [0.1–2.4 keV]	1.28 ± 0.04	1.39 ± 0.08	0.76 ± 0.06
z	0.25 ± 0.02	0.46 ± 0.05	1.27 ± 0.12
$\log \nu_r L_{\nu_r}$	41.51 ± 0.07	43.65 ± 0.16	44.93 ± 0.13
$\log \nu_o L_{\nu_o}$	44.66 ± 0.06	45.49 ± 0.12	46.35 ± 0.11
$\log \nu_x L_{\nu_x}$	44.62 ± 0.08	44.52 ± 0.15	45.89 ± 0.11
α_{ro}	0.36 ± 0.01	0.56 ± 0.02	0.66 ± 0.01
α_{ox}	1.03 ± 0.02	1.38 ± 0.02	1.21 ± 0.02
α_{rx}	0.59 ± 0.01	0.84 ± 0.01	0.85 ± 0.01

Table 3. Average values of X-ray spectral indices, redshifts, νL_ν luminosities in different bands and broad band spectral indices. The listed errors are weighted errors.

4.1. Histograms

The distribution of spectral indices, redshifts and luminosities are shown by the histograms in Fig. 1 – Fig. 9. In the figure captions we give the probability, according to the Kolmogorov-Smirnov (KS) test, that two distributions are drawn from the same parent population, comparing HBLs and LBLs, HBLs and FSRQs, LBLs and FSRQs.

The mean values of the plotted quantities are listed in Table 3.

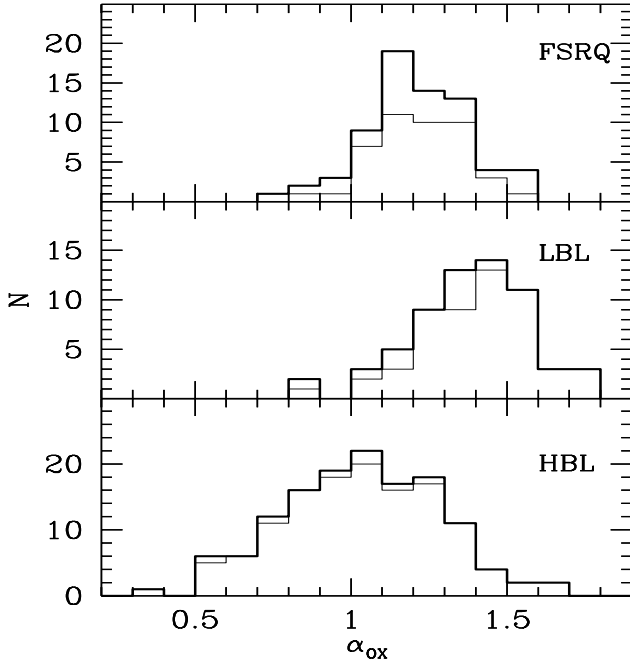


Fig. 8. Distribution of the broad band optical–X-ray spectral index for the three subclasses. Fluxes have been K-corrected as explained in the text. Thick solid lines refer to the entire sample, while thin solid lines refer to sources with only *ROSAT* data. KS test results (for the entire sample): $P = 5 \times 10^{-17}$ for HBL–LBL; 10^{-5} for HBL–FSRQ; 10^{-8} for LBL–FSRQ.

4.1.1. Spectral indices

The distributions of the energy spectral indices (Fig. 1 and Fig. 2) show that for FSRQ we have an average value less than unity in both energy ranges. This suggests that for this subclass of blazars we are observing only the inverse Compton component in the entire X-ray band, from 0.1 to 10 keV. For HBL, instead, the average energy spectral index is greater than unity, indicating that we are observing the synchrotron component after its peak. On average, LBL show a flattening going from the soft to the hard X-ray bands.

These results suggest that both the soft and the hard X-ray bands are dominated by the inverse Compton process in FSRQs and by the synchrotron process in HBL, while in LBL we have the synchrotron flux dominating in the soft band and the flatter Compton component emerging at higher X-ray energies.

4.1.2. Redshift

While the redshifts of FSRQs are quite uniformly distributed up to a value of $\simeq 3$, BL Lacs have redshifts lower than 1 (and HBL have lower redshifts than LBL, see Fig. 3). There is no significant difference between the redshift distributions of sources observed in the hard and in the soft X-ray bands. Of the sources in our sample,

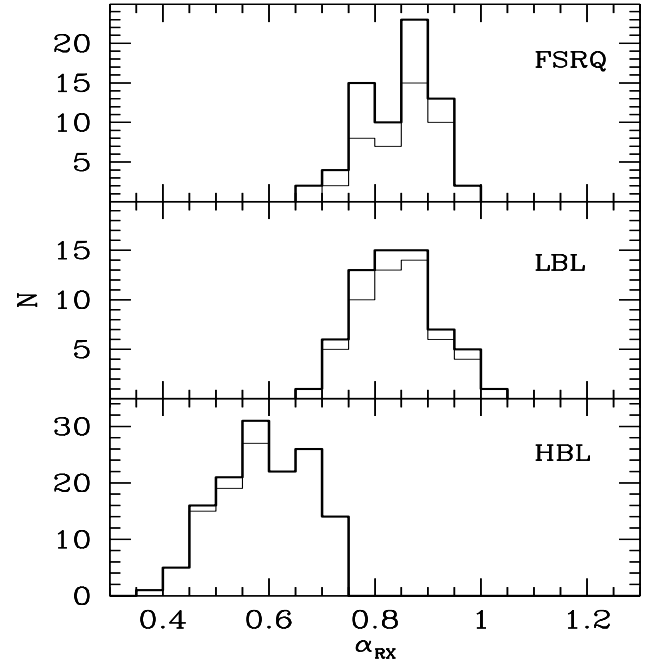


Fig. 9. Distribution of the broad band radio–X-ray spectral index for the three subclasses. Fluxes have been K-corrected as explained in the text. Thick solid lines refer to the entire sample, while thin solid lines refer to sources with only *ROSAT* data. KS test results (for the entire sample): $P = 8 \times 10^{-39}$ for HBL–LBL; 5×10^{-40} for HBL–FSRQ; 0.7 for LBL–FSRQ.

about 25% have no measured redshift (38 HBL and 17 LBL). This incompleteness, even if not severe, could bias the shown redshift distribution of HBLs towards the lower part (since larger redshifts are more difficult to measure).

4.1.3. Luminosities

From the radio, optical and 1 keV monochromatic fluxes we have calculated the “ νL_ν ” luminosities in the corresponding bands. The distributions of radio and optical luminosities (Fig. 4 and Fig. 5) show a continue variation in the three subclasses of blazar: HBLs are the least powerful sources, and FSRQs are the most luminous objects. this is more pronounced in the radio than in the optical band. The X-ray luminosities of HBLs and LBLs are very similar (Fig. 6), while FSRQs are more luminous by a factor of 10.

4.1.4. Broad band indices

Also the broad band spectral index α_{ro} changes smoothly between the subclasses of blazar (Fig. 7). On average, it becomes steeper going from HBL to FSRQs. The optical to X-ray broad band index distribution (Fig. 8) is broader for HBL, with an average value smaller than for LBL and FSRQs. The spectral index α_{rx} (Fig. 9) is on average the

$\langle \log \nu_r L_{\nu_r} \rangle$	$\langle \log \nu_x L_{\nu_x} \rangle$ @4.47 keV	N _{sources}	α_x 2–10 keV
< 42	44.2	12	1.39 ± 0.21
42–43	44.5	5	1.19 ± 0.21
43–44	44.9	6	0.95 ± 0.11
44–45	45.8	6	0.68 ± 0.02
>45	47.0	11	0.58 ± 0.06

Table 4. Average values of the X-ray luminosity at 4.47 keV (νL_{ν} values) and average 2–10 keV spectral indices, for the sources in common with Fossati et al. 1998, for each radio luminosity bin.

same for FSRQs and LBLs, and obviously flatter (by definition) for HBLs.

5. The average SED

In Fig. 10 we show the sequence of average SEDs as published by F98, but including the [2–10 keV] averages spectral indices and fluxes. The latter have been constructed considering only the same samples considered by F98.

It can be seen that in general the 2–10 keV fluxes and spectral indices connect smoothly on the softer *ROSAT* data even if they are, on average, flatter than the latter. This is due to the emergence, in the hard X-ray band, of the inverse Compton component which is progressively more dominant as the luminosity increases.

For the average SED corresponding to the second lowest luminosity bin, there is a mismatch between the soft and hard X-ray data. By comparing the data of each source in common, we found that all 5 sources were bright when observed by ASCA or *BeppoSAX* than at the time of the *ROSAT* observations. We therefore believe that the mismatch is due to the variable nature of the objects and the small number of sources in this luminosity bin.

The average spectral indices of the objects in common with F98 are listed in Table 5, which also lists the average luminosities at 4.47 keV (the logarithmic mid point between 2 and 10 keV).

The continuous lines in Fig. 10 correspond to a simple parametric model derived by the one introduced by Fossati et al. (1998). We introduce minor modifications, adopted both to better represent our data at small luminosities and to follow a more physical scenario, in which the low power HBLs can be described by a pure synchrotron–self Compton model (see e.g. Ghisellini et al., 1998). We remind the reader here of the key assumptions of the F98 parametric model:

- The observed radio luminosity $L_R = (\nu L_{\nu})|_{5\text{GHz}}$ is assumed to be linearly proportional to the bolometric luminosity, and related to the location of the synchrotron peak through:

$$\nu_s \propto L_R^{-\eta} \quad (1)$$

where $\eta = 1.8$ for $L_R < 3 \times 10^{42}$ erg s⁻¹ and $\eta = 0.6$ for $L_R > 3 \times 10^{42}$ erg s⁻¹.

- The ratio between the Compton and the synchrotron peak frequencies is constant: $\nu_c/\nu_s = 5 \times 10^8$ for all luminosities.
- The ratio between the power of the inverse Compton and the radio powers is constant: $L_c/L_R = 3 \times 10^3$ for all luminosities.
- The ratio between the radio and X-ray (at 1 keV) Compton luminosity is fixed.

The SED is then constructed assuming for the synchrotron component a flat ($\propto \nu^{-0.2}$) radio spectrum connecting to a parabola (in log–log space) peaking at ν_s . The junctions between the power law and the parabola is continuous. For the inverse Compton spectrum it is assumed that an initial power law of index $\alpha = 0.6$ ends in another parabola peaking at ν_c .

We modified the Fossati et al. (1998) description in the following way:

- We changed the values of η , assuming $\eta = 1.2$ and 0.4 for L_R smaller and greater than 10^{43} erg s⁻¹.
- The ratio ν_c/ν_s is assumed to be constant with the same value as before for $L_R > 10^{43}$ erg s⁻¹, but for smaller radio luminosity we set:

$$\frac{\nu_c}{\nu_s} = 5 \times 10^8 L_{R,43}^{-0.4} \quad (2)$$

- Below $L_R < 10^{43}$ erg s⁻¹ we assume that the synchrotron and Compton peaks have the same luminosities. For greater L_R we assumed, as before, $L_c/L_R = 3 \times 10^3$.

The spectra predicted by this new parameterization are shown in Fig. 10 as thin solid lines. As anticipated, the assumptions described above have a physical motivation. In fact, for low luminosity sources, we have evidences that the seed photons producing the Compton spectrum are the locally produced synchrotron ones, with no or negligible contributions from seed photons produced externally to the jet (e.g. from the Broad Line Region). In this case:

- i) The ratio ν_c/ν_s increases with ν_s as long as the scattering process is in the Thomson regime, and decreases with ν_s in the Klein Nishina regime.
- ii) On average, the BL Lacertae objects detected by EGRET with $L_R < 10^{43}$ erg s⁻¹ have roughly the same synchrotron and Compton components.
- iii) The radio luminosity $L_R = 10^{43}$ erg s⁻¹ may corresponds to the power for which emission lines and/or external seed photons becomes important for the formation of the inverse Compton spectrum (see e.g. Ghisellini et al., 1998).

6. Correlations

In order to see if the proposed parameterization of the average SED of blazars (constructed on the basis of a subsample of the sources in our catalogue) can account for

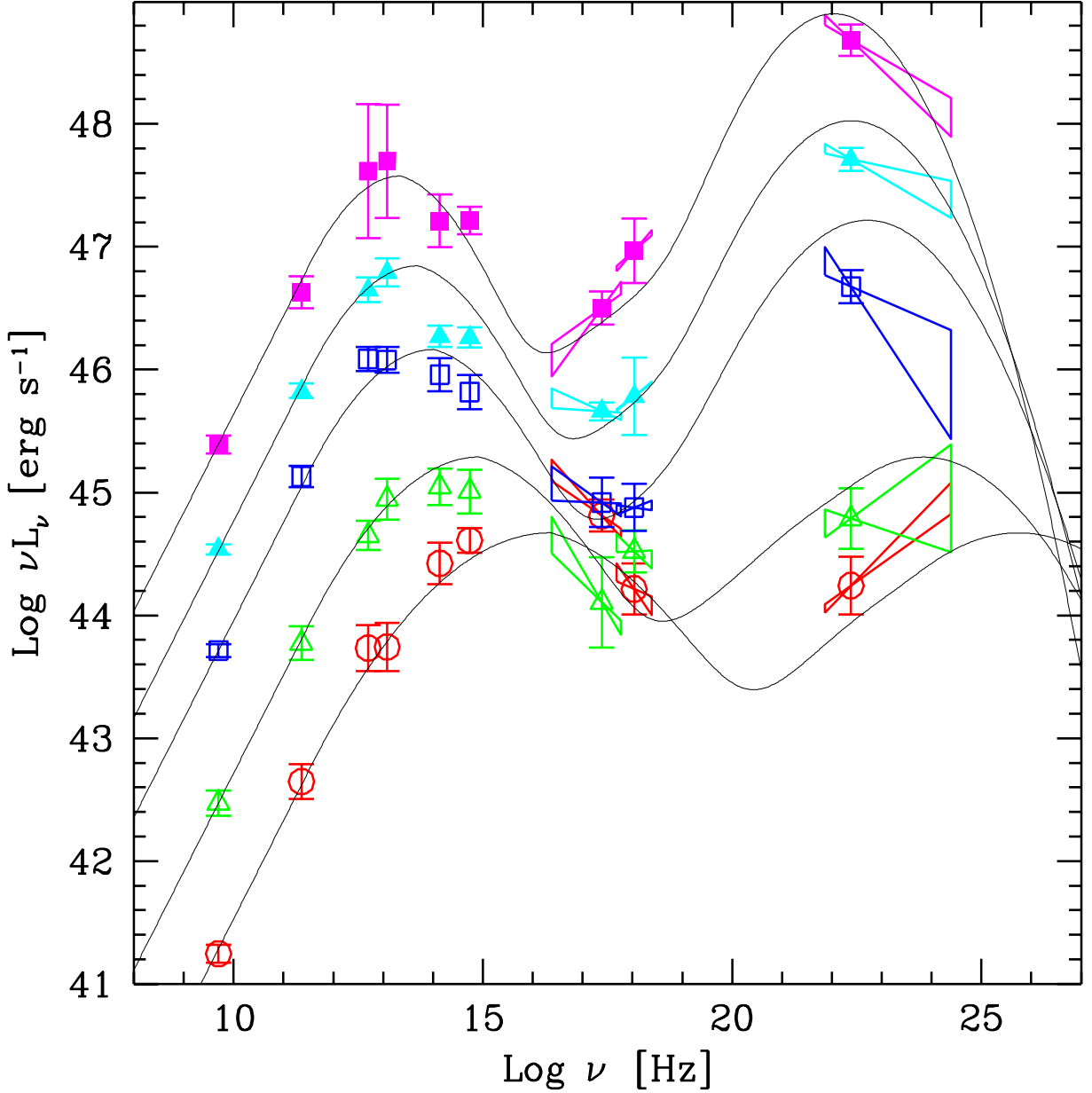


Fig. 10. The average SED of the blazars studied by Fossati et al. (1998), including the average values of the hard X-ray spectra. The thin solid lines are the spectra constructed following the parameterization proposed in this paper.

the general properties of all the blazars in our catalogue, we have investigated the correlations between the X-ray spectral index (both hard and soft) with the radio and X-ray luminosities and with the broad band spectral indices. We have then considered the correlations between broad band indices. The results are shown in Fig. 12–18 (solid line), where we have superposed the relations predicted by the new parameterization.

In Fig. 11 and Fig. 12 we show the hard and soft X-ray indices as a function of the radio and X-ray luminosity for all sources, and compare these data with the model

expectations. Note that the latter have been constructed to describe the *average* properties of blazars, whatever the scatter around it. Bearing this in mind, we can consider the description of the model quite satisfactorily.

In Fig. 13 we show the hard and soft X-ray indices as a function of the broad band index α_{rx} . The model well describes the small α_{rx} part (corresponding to HBLs), but fails to describe the X-ray flattest sources with the steeper value of α_{rx} . This is due to two reasons: i) the slope of the power law of the Compton component is assumed to be $\alpha = 0.7$, so that flatter indices are not possible; ii) the

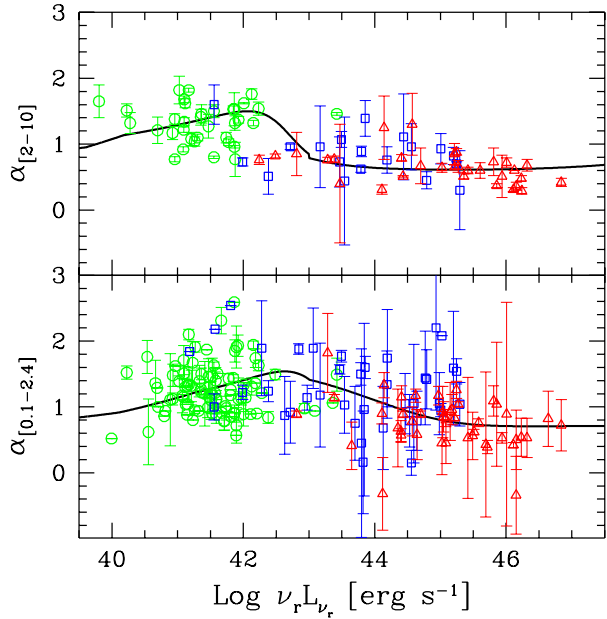


Fig. 11. Soft and hard X-ray spectral index vs. the radio luminosity. Circles: HBL, Squares: LBL, Triangles: FSRQs.

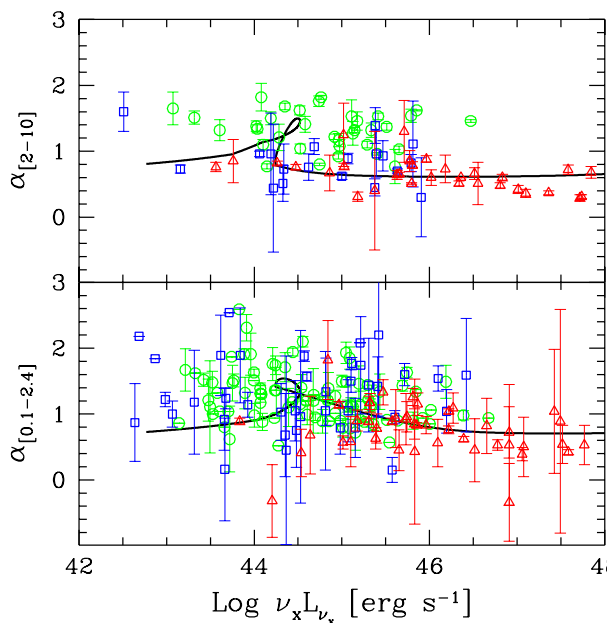


Fig. 12. Soft and hard X-ray spectral index vs. the X-ray luminosity. Circles: HBL, Squares: LBL, Triangles: FSRQs.

ratio between the radio and the 1 keV Compton luminosity is fixed for all sources. This results in a saturated value of $\alpha_{rx} \sim 0.85$, occurring when the Compton component dominates at 1 keV (i.e. for powerful sources).

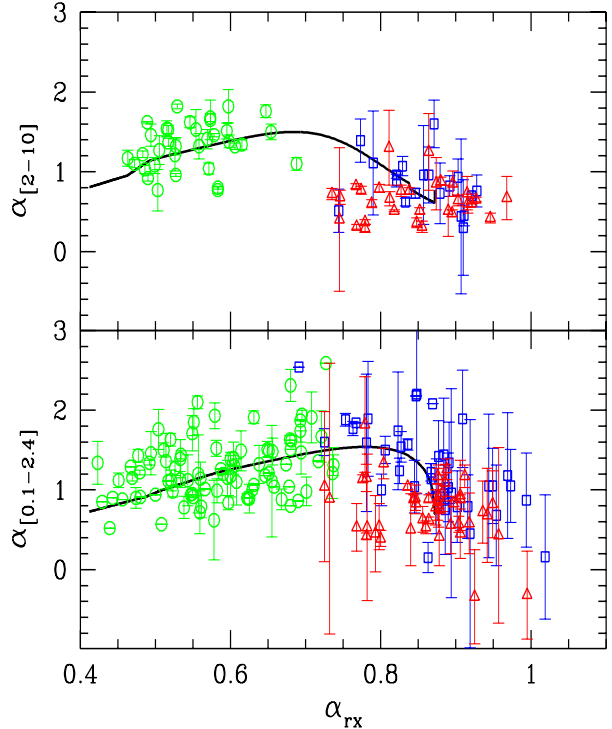


Fig. 13. Soft and hard X-ray spectral index vs. the broad band radio to X-ray index. Circles: HBL, Squares: LBL, Triangles: FSRQs.

In Fig. 14 and Fig. 15 we show α_X as a function of α_{ro} and α_{ox} : the average properties are well described by the model.

In Fig. 16, we show the “classic” $\alpha_{ro}-\alpha_{ox}$ diagram for the two subsamples of sources. Note that the model well describes all the data but those sources with the largest values of α_{ox} , corresponding to “transition” sources between the LBLs and FSRQ.

Fig. 17, Fig. 18: note that HBL are well separated from the other classes of blazars. Note also that the model, by construction, has an asymptotic limit for α_{rx} , whose value therefore saturates at $\alpha_{rx} \simeq 0.85$.

7. Discussion

The large database of X-ray spectra of blazars we have collected has allowed to test the blazar sequence scheme aiming to unify the different behaviors of blazars on the basis of a single parameter, i.e. the bolometric observed luminosity. We have found that the proposed parameterization can account for the average properties of the blazars in our sample, even if the scatter around the predicted average quantities is sometimes large.

We confirm, on a statistical basis, that more powerful blazars emit the X-rays by the inverse Compton process, while in less powerful objects the dominant mechanism is synchrotron, and the transition is smooth, with LBL possibly showing both contributions.

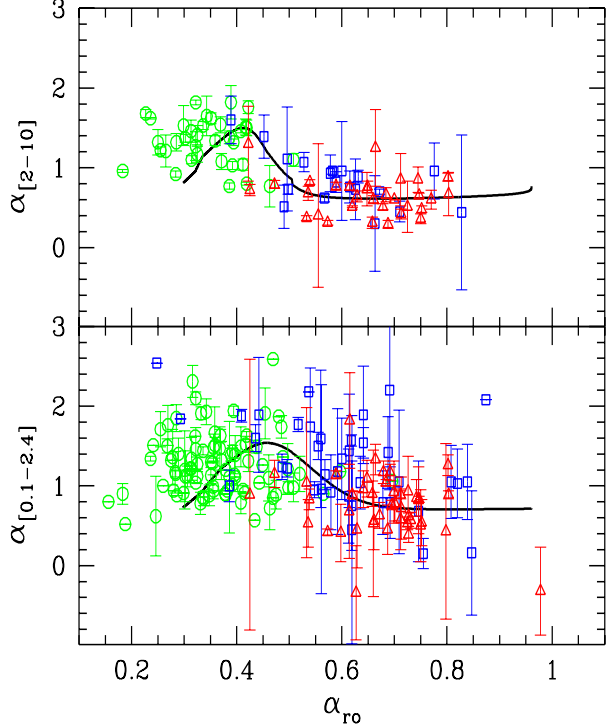


Fig. 14. Soft and hard X-ray spectral index vs. the broad band radio to optical index. Circles: HBL, Squares: LBL, Triangles: FSRQs.

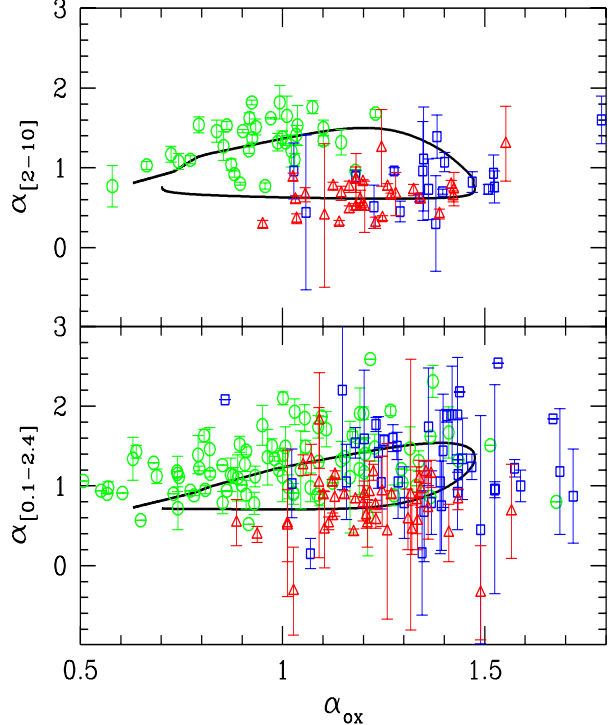


Fig. 15. Soft and hard X-ray spectral index vs. the broad band optical to X-ray index. Circles: HBL, Squares: LBL, Triangles: FSRQs.

The Fossati et al. (1998) parameterization scheme to reproduce the blazar SED is able to fit also our new hard X-ray data and the correlations between broad band indices of the sources in our sample. However, we propose to slightly change this parameterization especially for the low power objects (i.e. the HBLs), in line with the idea that HBLs are characterized by a pure synchrotron self-Compton spectrum, without extra contributions produced by non locally produced seed photons.

In this paper, and in Fossati et al. (1998), the power law relation between the synchrotron peak frequency and the radio luminosity changes slope at some critical radio power, of the order of $3-10 \times 10^{42}$ erg s $^{-1}$. This agrees with the absence of broad emission lines in these objects. It has still to be proven, however, if the non visibility of emission lines in low power objects is due to a genuine lack of emitting clouds, or is due to a weak ionizing continuum. If the latter hypothesis is true, then we expect that the broad line region indeed exists, but at smaller radii than in more powerful objects. In this case, the lack of the external Compton component is not due to the lack of external photons, but possibly to the fact that the dissipation region in these sources is beyond the broad line region: in this case the corresponding energy density of line photons is seen, in the comoving frame of the blob, depressed by the square of the bulk Lorentz factor.

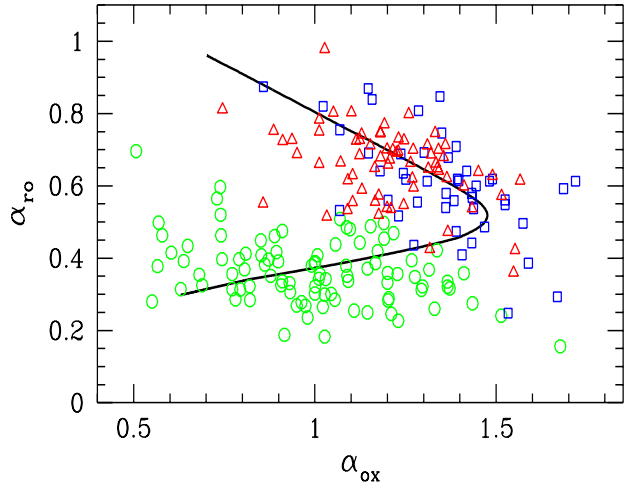


Fig. 16. Radio to optical vs. optical to X-ray broad band indices. Circles: HBL, Squares: LBL, Triangles: FSRQs.

Acknowledgements. We thank the anonymous referee for useful suggestions and Luigi Costamante for discussions. This research made use of the NASA/IPAC Extragalactic Database (NED) which is operated by the Jet Propulsion Laboratory, Caltech, under contract with the National Aeronautics and Space Administration. We acknowledge financial support from the MURST.

IAU Name	z	F_R (Jy)	Ref.	F_O (mJy)	Ref.	F_X (μ Jy)	Ref.	Γ	err	Ref.	Type	Ref.	Sat
0014+813	3.366	0.551	Ca97	0.910	Ca97	0.350 0.430	Ca97 Ca97	1.890 1.720	1.700 0.070	Ca97	3	Ca97	RO
0016+731	1.781	1.750	NED	0.060	NED	0.050	Sa97b	1.430	1.100	Sa97b	3	Gh93	RO
0038-020	1.178	0.581	NED	0.030	NED	0.100	Wo90	1.400	1.100	Wo90	3	Wo90	EI
0045+214	...	0.043	NED	0.310	NED	0.450	Br97	2.160	0.250	Br97	1	Br97	RO
0048-097	0.200	2.743	Fo98	1.750	Fo98	0.420 0.770	Pa98 Pa99	1.730 2.570	0.380 0.070	Pa98 Pa99	2	Gh93	SA
0109+182	...	0.077	NED	1.440	NED	1.180	LM99	1.940	—	LM99	1	LM99	RO
0110+418	0.096	0.036	NED	0.390	NED	0.300	Br97	2.110	0.700	Br97	1	Br97	RO
0112-017	1.365	1.200	Kh81	0.230	NED	0.150	Wo90	1.570	1.000	Wo90	3	Wo90	EI
0112+227	...	0.257	NED	2.220	NED	0.160	LM99	2.960	—	LM99	2	LM99	RO
0113+2504	...	0.031	NED	0.120	NED	0.710	Br97	1.840	0.370	Br97	1	Br97	RO
0118-272	0.557	1.284	Fo98	1.560	Fo98	0.280	Fo98	2.740	0.740	Fo98	2	NED	RO
0120+340	0.272	0.034	NED	3.600	NED	2.420 6.260	Cs00 Br94	1.960 1.900	0.020 0.130	Cs00 Br94	1	Br94	SA
0122+0903	0.339	0.001	Pa95	0.050	Pa95	0.030	Pe96	1.620	0.500	Pe96	1	Pe96	RO
0133+388	...	0.053	NED	4.590	NED	2.390	LM99	2.160	—	LM99	1	LM99	RO
0133+476	0.859	2.920	Fo98	0.470	Fo98	0.300	Fo98	1.920	0.390	Fo98	3	Gh93	RO
0145+138	0.125	0.005	Fo98	0.260	Fo98	0.220	BSMc	2.320	0.160	BSMc	1	BSMc	SA
0152+017	0.080	0.058	NED	0.900	NED	0.470	Br97	2.480	0.170	Br97	1	Br97	RO
0156+1032	...	0.044	NED	0.950	NED	0.630	Br97	1.730	0.630	Br97	1	Br97	RO
0158+003	0.299	0.011	Fo98	0.230	Fo98	1.210 1.030	Fo98 Wo98	2.460 2.270	0.270 0.180	Fo98 Wo98	1	NED	RO
0159+0835	...	0.071	NED	0.120	NED	0.270	Br97	2.360	0.480	Br97	1	Br97	RO
0202+149	0.405	2.400	Co97	0.020	Co97	0.060	Co97	0.680	0.550	Co97	3	NED	RO
0205+3509	0.318	0.004	Pa95	0.180	Pa95	0.150 0.550	Pe96 Wa99	2.710 2.220	0.220 0.040	Pe96 Wa99	1	Pe96	RO
0208-512	1.003	3.311	Fo98	0.590	Fo98	0.610 1.200	Fo98 Ku98	2.040 1.660	0.040 0.090	Fo98 Ku98	3	IT90	RO
0212+735	2.370	2.198	Fo98	0.450	Fo98	0.260	Fo98	0.660	0.590	Fo98	3	Gh93	RO
0214+517	0.049	0.271	NED	1.550	NED	1.600	LM99	2.040	—	LM99	1	LM99	RO
0219+428	0.444	1.040	Fo98	4.550	Fo98	0.720 1.560	Sa94 Fo98	2.390 2.600	0.270 0.170	Sa94 Fo98	2	Gh93	EX
						3.460	Wo90	2.620	0.850	Wo90		Ro	
0224+014	...	0.009	Br97	0.120	NED	3.360	Br97	1.900	0.110	Br97	1	Br97	RO
0235+164	0.940	3.336	Fo98	2.580	Fo98	0.150 0.270	Go95	1.750	0.730	Go95	2	Gh93	EX
						1.150	Fo98	2.590	0.860	Fo98		Ro	
						1.510	Wo90	3.250	2.100	Wo90		EI	
0237-233	2.223	3.520	Kh81	0.810	NED	0.310 0.390	Wo90 Re97	1.620 1.680	1.250 0.060	Wo90 Re97	3	Wo90	EI
						0.390	Re97	1.680	0.060	Re97		AS	
0250+172	...	0.035	NED	2.060	NED	0.730	LM99	2.020	—	LM99	1	LM99	RO
0257+3429	0.245	0.010	Pa95	0.140	Pa95	0.020	Pe96	2.670	0.320	Pe96	1	Pe96	RO
0301-243	...	0.397	NED	0.980	NED	0.270	La96	2.680	0.310	La96	2	La96	RO
0316+090	...	0.045	NED	1.160	NED	0.020	LM99	4.280	—	LM99	2	LM99	RO
0317+1834	0.190	0.017	Pa95	0.210	Pa95	0.170 3.060	Pe96 Sa94	2.320 1.800	0.240 0.200	Pe96 Sa94	1	Wo98	RO
						2.050	Wo98	2.080	0.100	Wo98		EX	
0323+022	0.147	0.042	Fo98	0.900	Fo98	6.810 4.000	Wo90 Sa94	2.160 2.730	0.230 0.100	Wo90 Sa94	1	Wo90	EI
						1.460	BSMc	2.410	0.120	BSMc		EX	
						0.730	Ku98	2.740	0.160	Ku98		SA	
						3.210	Fo98	2.270	0.090	Fo98		AS	
0331-365	0.308	0.009	VV93	0.240	NED	0.340	La96	2.200	0.490	La96	1	La96	RO
0332-403	1.445	2.600	Ca97	0.140	Ca97	0.140	Ca97	1.600	0.120	Ca97	3	Ca97	AS
0333+321	1.258	2.500	Ca97	0.520	Gh93	1.600 1.340	Ca97 Ku98	1.530 1.600	0.920 0.050	Ca97 Ku98	3	Gh93	RO
						2.320	Wo90	3.730	2.100	Wo90		EI	
						0.440	Go95	1.360	0.260	Go95		EX	
0347-121	0.188	0.009	Fo98	0.190	Fo98	2.050 2.560	Wo98 Fo98	2.170 2.120	0.100 0.090	Wo98 Fo98	1	Wo98	SA
						2.560	Fo98	2.120	0.090	Fo98		RO	

IAU Name	z	F_R (Jy)	Ref.	F_O (mJy)	Ref.	F_X (μ Jy)	Ref.	Γ	err	Ref.	Type	Ref.	Sat
0350-3712	0.165	0.017	VV93	0.590	NED	0.350	La96	2.170	0.260	La96	1	La96	RO
0403-132	0.571	2.889	Fo98	0.540	Fo98	0.400	Fo98	1.780	0.220	Fo98	3	IT90	RO
						0.490	Wo90	4.300	4.300	Wo90		EI	
0405-123	0.574	1.960	Fo98	5.170	Fo98	0.090	TW	1.760	0.090	TW	3	Sa97b	AS
						1.160	Fo98	2.150	0.170	Fo98		RO	
0406+121	1.020	0.746	Na96	0.120	NED	0.050	La96	1.790	0.450	La96	2	La96	RO
0414+009	0.287	0.070	Fo98	0.850	Fo98	5.220	Wo98	2.540	0.100	Wo98	1	Wo98	SA
						5.460	Sa94	2.150	0.070	Sa94		EX	
						4.690	Wo98	2.630	0.080	Wo98		RO	
						4.620	Ku98	2.620	0.040	Ku98		AS	
0419+1943	0.512	0.008	Pa95	0.030	Pa95	0.300	Pe96	1.720	0.270	Pe96	1	Pe96	RO
0420-014	0.915	3.720	Co97	0.340	Co97	0.370	Wo90	0.850	2.100	Wo90	3	Co97	EI
						0.280	TW	1.860	0.180	TW		AS	
0426-380	1.030	1.416	Fo98	0.230	Fo98	0.090	Fo98	3.200	1.250	Fo98	2	NED	RO
0430+052	0.033	7.526	NED	3.910	Gh93	3.240	Go95	1.760	0.070	Go95	3	Gh93	EX
0438-436	2.852	6.189	Fo98	0.410	Fo98	0.190	Ca97	1.420	0.060	Ca97	3	Ca97	AS
						0.150	Fo98	1.720	0.390	Fo98		RO	
0454+844	0.112	1.430	Fo98	1.050	Fo98	0.030	Fo98	1.870	0.590	Fo98	2	Gh93	RO
0502+675	...	0.032	Fo98	0.790	Fo98	8.510	Wo98	2.340	0.060	Wo98	1	Wo98	SA
						7.740	Br94	1.910	0.290	Br94		RO	
0505+042	...	0.121	NED	0.960	NED	0.730	LM99	2.350	—	LM99	1	LM99	RO
0507-040	0.304	0.027	Fo98	0.110	Fo98	3.000	Sa94	1.770	0.260	Sa94	1	NED	EX
0521-365	0.055	9.700	Co97	2.380	Co97	1.230	Wo90	2.140	1.650	Wo90	3	Gh93	EI
						2.120	Co97	1.890	0.050	Co97		RO	
						1.780	Sa94	1.850	0.330	Sa94		EX	
0528+134	2.060	3.980	Fo98	0.210	Fo98	1.590	Fo98	1.540	0.290	Fo98	3	Gh93	RO
						1.480	Ku98	1.580	0.050	Ku98		AS	
						0.310	Gh98b	1.480	0.040	Gh98b		SA	
						0.220	Br85	2.600	—	Br85		EI	
0537-441	0.896	4.755	Fo98	1.570	Fo98	0.400	Sa94	1.300	0.600	Sa94	2	Gh93	EX
						0.780	Fo98	2.040	0.330	Fo98		RO	
						0.170	Wo90	1.270	1.700	Wo90		EI	
0537-286	3.104	0.990	Ca97	0.040	Ca97	0.180	Ca97	1.360	0.060	Ca97	3	Ca97	AS
						0.170	Ca97	1.500	0.450	Ca97		RO	
0548-322	0.069	0.170	Fo98	1.370	Fo98	8.220	Ku98	1.960	0.020	Ku98	1	NED	AS
						9.590	Fo98	1.950	0.050	Fo98		RO	
						6.460	Gh99	2.040	0.070	Gh99		SA	
						7.710	Sa94	1.980	0.060	Sa94		EX	
						9.960	Wo90	1.690	0.120	Wo90		EI	
0556-3838	0.034	0.068	Pa95	0.530	Pa95	2.200	Ge96	2.520	0.100	Ge96	1	Ge96	RO
						1.730	Ge96	2.510	0.100	Ge96		AS	
0607+7108	0.267	0.018	Pa95	0.050	Pa95	0.030	Pe96	2.210	0.320	Pe96	1	Pe96	RO
0615+820	0.710	1.000	Kh81	0.470	NED	0.040	Sa97b	1.680	0.590	Sa97b	3	Gh93	RO
0637-752	0.651	5.849	Fo98	2.380	Fo98	1.060	Wo90	1.580	0.800	Wo90	3	Sa97b	EI
						3.760	Fo98	1.450	0.480	Fo98		RO	
						0.490	Ya98	1.640	0.070	Ya98		AS	
0642+449	3.400	1.204	NED	0.150	NED	0.120	Wo90	1.410	1.300	Wo90	3	Wo90	EI
0647+250	...	0.077	NED	3.710	NED	6.010	Br94	2.470	0.320	Br94	1	Br94	RO
0651+428	0.126	0.188	NED	0.770	NED	0.360	LM99	3.590	—	LM99	1	LM99	RO
0656+426	0.059	0.480	NED	0.890	NED	0.130	LM99	3.180	—	LM99	2	LM99	RO
0706+5913	0.125	0.080	NED	0.180	NED	1.830	Br94	2.150	0.220	Br94	1	Br94	RO
0716+714	0.300	1.150	Fo98	2.200	Fo98	0.990	Fo98	2.770	0.090	Fo98	2	Gh93	RO
						0.370	Ku98	2.070	0.120	Ku98		AS	
						0.500	Wo90	5.750	4.400	Wo90		EI	
0735+178	0.424	2.490	Fo98	1.660	Fo98	0.220	Fo98	2.340	0.510	Fo98	2	Gh93	RO
						0.290	Wo90	1.710	0.400	Wo90		EI	
						0.140	Ku98	1.760	0.200	Ku98		AS	
0736+017	0.191	1.999	Fo98	1.330	Fo98	0.370	Wo90	4.200	3.500	Wo90	3	IT90	EI
						0.640	Sa99	1.760	0.040	Sa99		AS	
						1.490	Fo98	2.820	0.600	Fo98		RO	

IAU Name	z	F_R (Jy)	Ref.	F_O (mJy)	Ref.	F_X (μ Jy)	Ref.	Γ	err	Ref.	Type	Ref.	Sat
0737+746	0.315	0.024	Fo98	0.650	Fo98	0.880 1.110	Wo98 Fo98	2.530 1.910	0.250	Wo98	1	Wo98	SA
0754+100	0.660	1.480	Pa95	3.640	Pa95	0.720	Sa94	2.110	0.650	Sa94	2	Sa94	EX
0804+499	1.433	2.050	Co97	0.390	Co97	0.170	Co97	1.560	0.360	Co97	3	Gh93	RO
0806+3504	0.082	0.180	NED	0.660	NED	0.740	Ba98	2.870	—	Ba98	1	Ba98	RO
0806+524	0.138	0.177	NED	3.150	NED	4.910	Br94	2.930	0.160	Br94	1	Br94	RO
0806+595	...	0.042	NED	1.410	NED	0.710	LM99	1.500	—	LM99	1	LM99	RO
0808+019	...	0.670	Pa95	0.480	Pa95	0.380	Wo90	1.920	1.400	Wo90	2	Wo90	EI
0812+026	...	0.071	NED	6.250	NED	1.850	Br97	2.160	0.110	Br97	1	Br97	RO
0814+425	0.258	3.500	Fo98	0.150	Fo98	0.050	Fo98	1.160	0.780	Fo98	2	IT91	RO
0820+225	0.951	1.977	Fo98	0.060	Fo98	0.050	Fo98	2.050	0.470	Fo98	2	NED	RO
0828+493	0.548	1.158	Fo98	0.130	Fo98	0.040	Fo98	1.680	0.630	Fo98	2	NED	RO
0829+046	0.180	2.105	Pa95	1.450	Pa95	0.400	Wo90	3.260	3.400	Wo90	2	Gh93	EI
0833+3300	0.671	0.004	Ba98	0.020	NED	0.370	Ba98	1.570	—	Ba98	1	Ba98	RO
0836+710	2.170	2.590	Fo98	1.060	Fo98	1.270 2.260 1.600	Ca97 Tv99 Fo98	1.320 1.310 1.420	0.030 0.030 0.040	Ca97 Tv99 Fo98	3	Gh93	AS
0847+115	0.198	0.022	Br97	0.900	NED	1.980	Br97	2.500	0.090	Br97	1	Br97	RO
0850+443	...	0.075	NED	0.090	NED	0.190	Br97	2.800	0.300	Br97	1	Br97	RO
0851+202	0.306	2.173	Fo98	2.640	Fo98	0.930 2.240 0.370 0.730	Fo98 Sa94 Pa99 Ku98	2.500 2.370 1.710 1.620	0.170 0.100 0.240 0.050	Fo98 Sa94 Pa99 Ku98	2	Gh93	RO
0855+143	1.408	0.890	Br85	0.030	NED	0.320	Br85	2.000	—	Br85	3	NED	EI
0906+430	0.670	1.300	Fo98	0.160	Fo98	0.110	Fo98	1.570	0.100	Fo98	3	Gh93	RO
0906+311	0.274	0.087	NED	2.050	NED	0.650	Ba98	2.210	—	Ba98	1	Ba98	RO
0912+297	...	0.228	Na96	1.000	Pa95	1.060 0.510 0.580	Pa95 Wo90 La96	2.250 1.760 2.310	0.140 0.700 0.240	Pa95 Wo90 La96	1	NED	SA
0913+5251	0.190	0.067	NED	0.060	NED	0.590	Ba98	2.180	—	Ba98	1	Ba98	RO
0917+449	2.180	1.030	Co97	0.070	Co97	0.470	Co97	1.390	0.100	Co97	3	NED	RO
0922+7459	0.638	0.003	Pa95	0.050	Pa95	0.150	Pe96	1.780	0.140	Pe96	1	Pe96	RO
0923+392	0.699	8.101	Fo98	0.430	Fo98	0.620 0.370 0.880	Fo98 Wo90 Sa99	2.260 1.360 1.880	0.130 0.190 0.050	Fo98 Wo90 Sa99	3	Gh93	RO
0925+5026	...	0.558	NED	1.520	NED	0.120	Br97	2.300	0.390	Br97	2	Br97	RO
0927+500	0.188	0.015	Na96	0.500	NED	4.000	Ba98	1.880	—	Ba98	1	Ba98	RO
0945+408	1.252	1.450	NED	0.380	NED	0.110	Sa97b	1.960	0.230	Sa97b	3	IT91	RO
0950+445	0.207	0.003	Fo98	0.120	Fo98	0.290	Fo98	2.760	0.250	Fo98	1	NED	RO
0952+656	...	0.027	LM99	0.800	NED	0.150	LM99	2.230	—	LM99	1	LM99	RO
0954+556	0.909	2.169	Fo98	0.430	Fo98	0.100	Fo98	2.170	0.140	Fo98	3	IT91	RO
0954+658	0.367	1.589	Fo98	1.720	Fo98	0.160	Fo98	1.960	1.310	Fo98	2	Gh93	RO
1008+4705	0.343	0.004	Na96	0.090	NED	1.510	Ba94	2.340	0.270	Ba94	1	Ba94	RO
1009+427	0.364	0.056	NED	0.960	NED	1.110	Br97	1.840	0.090	Br97	1	Br97	RO
1011+496	0.200	0.286	Fo98	1.620	Fo98	2.150	Fo98	2.490	0.080	Fo98	1	NED	RO
1019+5139	0.141	0.002	Pa95	0.210	Pa95	0.790	Pe96	1.520	—	Pe96	1	Pe96	RO
1028+511	0.361	0.044	Fo98	0.800	Fo98	3.350 4.070 4.480 4.940	TW TW TW BSMc	2.530 2.490 2.590 2.410	0.050 0.040 0.050 0.040	TW TW TW BSMc	1	NED	AS
1034-293	0.312	1.510	Kh81	1.110	NED	0.240	Sa97b	1.410	0.360	Sa97b	3	Gh93	RO
1034-293	0.312	1.510	NED	0.930	Gh93	0.160	Wo90	0.660	1.800	Wo90	2	Gh93	EI
1037+571	...	0.088	NED	0.770	NED	0.380	Sb99	2.420	0.250	Sb99	1	Br97	SA
1039+811	1.260	1.140	Kh81	0.980	NED	0.180	Sa97b	1.830	0.130	Sa97b	3	Gh93	RO
1040+123	1.029	1.560	Kh81	0.470	Gh93	0.100	Wo90	1.450	0.900	Wo90	3	Gh93	EI
1047+546	...	0.004	Br97	0.040	NED	0.070	Br97	1.630	0.370	Br97	1	Br97	RO
1053+494	0.140	0.019	LM99	0.430	NED	0.090	LM99	2.620	—	LM99	1	LM99	RO
1055+018	0.888	3.470	Fo98	0.400	Fo98	0.210	Fo98	1.930	0.440	Fo98	3	NED	RO

IAU Name	z	F_R (Jy)	Ref.	F_O (mJy)	Ref.	F_X (μ Jy)	Ref.	Γ	err	Ref.	Type	Ref.	Sat
1055+567	0.144	0.260	NED	1.810	NED	0.470	Br97	2.310	0.130	Br97	1	Br97	RO
						2.190	Sb99	2.760	0.080	Sb99			AS
						1.080	Sb99	2.780	0.250	Sb99			SA
1101+384	0.031	0.722	Fo98	16.970	Fo98	58.370	Fo98b	2.820	0.030	Fo98b	1	Gh93	SA
						23.850	Ku98	2.970	0.020	Ku98			AS
						36.100	Fo98	3.100	0.080	Fo98			RO
1101-232	0.186	0.066	Fo98	0.640	Fo98	10.230	Wo98	2.030	0.050	Wo98	1	Wo98	SA
						11.200	Wo98	2.430	0.080	Wo98			RO
						19.630	Wo90	2.310	0.180	Wo90			EI
						17.740	Sa94	2.500	0.170	Sa94			EX
1112+3452	0.212	0.004	Ba98	0.060	NED	0.810	Ba98	2.290	—	Ba98	1	Ba98	RO
1114+2030	...	0.074	NED	3.210	NED	7.310	Br97	1.900	0.050	Br97	1	Br97	RO
1118+424	0.124	0.035	Fo98	0.560	Fo98	1.830	BSMc	2.620	0.070	BSMc	1	BSMc	SA
						0.670	LM99	2.300	—	LM99			RO
1133+6753	0.135	0.048	NED	0.450	NED	3.230	Br94	2.390	0.240	Br94	1	Br94	RO
1133+704	0.046	0.274	Fo98	4.140	Fo98	4.870	Sa94	2.340	0.060	Sa94	1	NED	EX
						9.200	Wo90	1.970	0.170	Wo90			EI
						2.620	Fo98	2.510	0.100	Fo98			RO
						2.610	Wo98	2.470	0.090	Wo98			SA
1144-379	1.048	2.779	Fo98	0.800	Fo98	0.140	Pa98	1.700	0.030	Pa98	2	IT90	SA
						0.410	Pa99	2.540	0.190	Pa99			RO
1146-037	0.341	0.354	NED	0.630	NED	0.580	Wo90	1.390	0.710	Wo90	3	Wo90	EI
1147+245	0.200	1.385	Fo98	1.200	Fo98	0.300	Go95	1.960	0.620	Go95	2	Gh93	EX
						0.040	Fo98	2.180	0.790	Fo98			RO
1148+592	...	0.134	NED	0.480	NED	0.270	Br97	1.620	0.230	Br97	1	Br97	RO
1150+497	0.334	0.699	NED	0.560	NED	0.550	Sa97b	2.140	0.050	Sa97b	3	Sa97b	RO
						0.630	Sa99	1.770	0.050	Sa99			AS
1150+812	1.250	1.180	Kh81	0.180	NED	0.090	Sa97b	1.450	0.310	Sa97b	3	Gh93	RO
1156+295	0.729	1.543	NED	6.640	NED	0.440	Sa94	2.300	0.470	Sa94	3	NED	EX
1206+416	...	0.515	NED	1.150	NED	0.100	LM99	2.100	—	LM99	2	LM99	RO
1207+3945	0.615	0.006	Pa95	0.080	Pa95	0.280	Pe96	2.130	0.100	Pe96	1	Pe96	RO
1212+0748	0.130	0.094	NED	1.550	NED	0.620	Br97	1.880	0.130	Br97	1	Br97	RO
1215+303	0.237	0.445	Fo98	3.110	Fo98	0.490	Fo98	2.880	0.080	Fo98	2	Gh93	RO
						0.590	Wo90	2.420	0.900	Wo90			EI
1217+348	...	0.355	NED	0.550	NED	0.100	La96	1.980	0.710	La96	2	La96	RO
1217+023	0.240	0.698	NED	0.890	NED	0.780	Wo90	1.700	0.350	Wo90	3	Wo90	EI
1218+304	0.130	0.056	Fo98	1.390	Fo98	7.510	Sa94	2.460	0.140	Sa94	1	NED	EX
						10.050	Fo98	2.220	0.030	Fo98			RO
1219+285	0.102	0.981	Fo98	3.150	Fo98	1.010	Wo90	3.750	1.500	Wo90	2	Gh93	EI
						0.400	Fo98	2.240	0.160	Fo98			RO
						1.790	Ta00	1.510	0.270	Ta00			SA
1220+345	...	0.355	NED	0.550	NED	0.060	LM99	1.980	—	LM99	2	LM99	RO
1221+2452	0.218	0.026	Pa95	0.330	Pa95	0.090	Pe96	2.470	0.270	Pe96	1	Pe96	RO
1225+317	2.200	0.342	NED	1.630	NED	0.180	Wo90	1.720	1.000	Wo90	3	Wo90	EI
1226+023	0.158	42.861	Fo98	27.640	Fo98	20.420	Ku98	1.510	0.010	Ku98	3	Gh93	AS
						12.270	Fo98	1.890	0.050	Fo98			RO
						7.600	Go95	1.580	0.030	Go95			EX
						11.150	Wo90	1.340	0.170	Wo90			EI
						1.960	Or98	1.570	0.050	Or98			SA
1229+6430	0.164	0.042	Pa95	0.630	Pa95	1.210	Pe96	1.990	0.150	Pe96	1	Pe96	RO
1230+2517	0.135	0.425	NED	2.220	NED	0.320	Ba94	2.890	0.720	Ba94	2	Ba94	RO
1235+6315	0.297	0.007	Pa95	0.130	Pa95	0.060	Pe96	2.910	0.080	Pe96	1	Pe96	RO
1237+3020	0.700	0.003	Na96	0.010	NED	0.960	Ba98	1.850	—	Ba98	1	Ba98	RO
1239-143	...	0.042	NED	0.290	NED	1.620	Ba94	2.580	0.570	Ba94	1	Ba94	RO
1242+3440	...	0.008	Na96	0.060	NED	0.320	Ba98	1.930	—	Ba98	1	Ba98	RO
1246+586	...	0.414	NED	9.450	NED	0.500	Ba98	2.420	—	Ba98	2	Ba98	RO
1252+119	0.871	1.140	Kh81	0.800	NED	0.140	Wo90	1.070	1.300	Wo90	3	Wo90	EI
1253-055	0.536	14.950	Fo98	1.660	Fo98	1.340	Fo98	1.830	0.040	Fo98	3	Gh93	RO
						0.850	Ma98	1.650	0.030	Ma98			SA
						1.500	Ku98	1.650	0.060	Ku98			AS
						0.630	Wo90	1.550	0.270	Wo90			EI

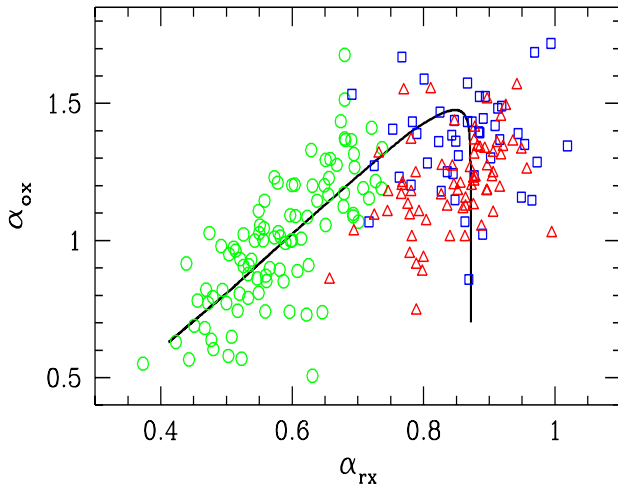
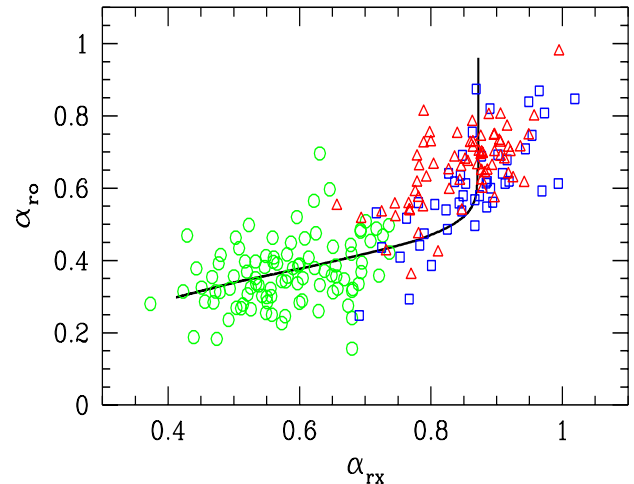
IAU Name	z	F_R (Jy)	Ref.	F_O (mJy)	Ref.	F_X (μ Jy)	Ref.	Γ	err	Ref.	Type	Ref.	Sat
1255+244	0.141	0.077	Pa95	2.510	Pa95	1.450	Gr96	2.400	0.200	Gr96	1	Gr96	RO
1303+5056	0.688	0.001	Ba98	0.030	NED	0.830	Ba98	1.940	—	Ba98	1	Ba98	RO
1308+326	0.997	1.832	Fo98	1.580	Fo98	0.110	TW	1.990	0.420	TW	2	Gh93	AS
						0.090	TW	1.740	0.250	TW			AS
						0.150	Co95	1.950	0.100	Co95			RO
1312-423	0.105	0.019	Pa95	0.830	Pa95	1.520	Wo98	2.210	0.200	Wo98	1	Wo98	SA
1324+5739	0.115	0.042	NED	0.950	NED	0.330	Ba98	2.040	—	Ba98	1	Ba98	RO
1326+2933	0.431	0.006	Na96	0.050	NED	0.430	Ba98	2.110	—	Ba98	1	Ba98	RO
1332-295	0.513	0.011	Fo98	0.090	Fo98	0.340	Fo98	2.140	0.210	Fo98	1	NED	RO
1334-127	0.539	2.250	Kh81	0.600	NED	0.450	Sa97b	1.630	0.160	Sa97b	3	Gh93	RO
1353+5601	0.370	0.012	Na96	0.110	NED	0.390	Ba98	2.010	—	Ba98	1	Ba98	RO
1400+162	0.244	0.528	Pa95	0.510	NED	0.140	Wo90	1.550	1.100	Wo90	2	Gh93	EI
1402+042	0.344	0.020	Fo98	0.630	Fo98	1.200	Sa94	2.320	0.110	Sa94	1	NED	EX
						0.680	Fo98	2.850	0.170	Fo98			RO
1405+6554	0.364	0.015	Ba98	0.070	NED	0.310	Ba98	2.260	—	Ba98	1	Ba98	RO
1407+5954	0.495	0.017	Pa95	0.050	Pa95	0.040	Pe96	2.740	0.140	Pe96	1	Pe96	RO
1410+6100	0.384	0.033	Ba98	0.040	NED	0.410	Ba98	1.900	—	Ba98	1	Ba98	RO
1413+135	0.247	1.200	Pa95	0.040	NED	0.050	Wo90	0.600	1.500	Wo90	2	Wo90	EI
1415+485	...	0.035	NED	0.720	NED	0.040	LM99	2.400	—	LM99	2	LM99	RO
1415+259	0.237	0.054	Pa95	1.450	Pa95	4.280	Sa94	2.370	0.050	Sa94	1	NED	EX
						2.870	Br94	2.120	0.320	Br94			RO
1418+546	0.152	1.610	Fo98	1.910	Fo98	0.210	Wo90	1.480	0.650	Wo90	2	Wo90	EI
						0.300	Fo98	2.140	0.190	Fo98			RO
1421+582	0.638	0.050	Br94	0.120	NED	2.950	Br94	1.980	0.070	Br94	1	Br94	RO
1424+240	...	0.316	NED	1.090	NED	1.470	Sb99	2.780	0.040	Sb99	1	Gh93	AS
						1.260	La96	3.180	0.160	La96			RO
1426+428	0.129	0.030	NED	1.050	Sa97	13.420	Sa94	2.100	0.070	Sa94	1	NED	EX
						6.500	Sa97a	2.150	0.040	Sa97a			RO
						5.940	Ku98	2.170	0.030	Ku98			AS
						4.640	Gh99	1.920	0.040	Gh99			SA
1427+541	0.105	0.024	LM99	0.470	LM99	0.110	LM99	1.860	—	LM99	1	LM99	RO
1428+422	4.715	0.337	Fa97	0.020	Fa98	0.210	Fa98	1.290	0.050	Fa98	3	Fa98	AS
1437+398	...	0.063	NED	1.520	NED	1.190	LM99	2.550	—	LM99	1	LM99	RO
1437+5639	...	0.011	Na96	0.120	NED	0.300	Ba98	2.220	—	Ba98	1	Ba98	RO
1440+122	0.162	0.050	NED	0.570	NED	1.220	LM99	2.200	—	LM99	1	LM99	RO
1442+101	3.530	1.260	Kh81	0.280	NED	0.120	Wo90	2.000	1.300	Wo90	3	Wo90	EI
1443+6349	0.299	0.012	Pa95	0.050	Pa95	0.190	Pe96	2.100	0.290	Pe96	1	Pe96	RO
1448+361	...	0.029	LM99	1.140	NED	0.500	LM99	2.600	—	LM99	1	LM99	RO
1456+5048	0.480	0.274	NED	0.070	NED	2.560	Ba98	2.060	—	Ba98	1	Ba98	RO
1458+2249	0.235	0.030	Pa95	0.690	Pa95	0.110	Pe96	3.310	0.200	Pe96	1	Pe96	RO
1458+4832	0.539	0.003	Ba98	0.030	NED	0.800	Ba98	1.900	—	Ba98	1	Ba98	RO
1509+559	...	0.042	NED	0.950	NED	0.050	LM99	2.990	—	LM99	1	LM99	RO
1510-089	0.361	3.080	Fo98	1.090	Fo98	0.750	Sn97	1.310	0.070	Sn97	3	Gh93	AS
						0.500	Wo90	0.800	1.350	Wo90			EI
						0.830	Sa94	1.380	0.280	Sa94			EX
						0.490	Tv99	1.350	0.070	Tv99			SA
						0.740	Fo98	1.900	0.160	Fo98			RO
1514-241	0.049	2.000	Pa95	2.900	NED	0.620	Wo90	2.360	1.950	Wo90	2	Wo90	EI
1516+293	0.130	0.034	LM99	1.320	NED	0.190	LM99	2.320	—	LM99	1	LM99	RO
1517+656	...	0.038	Fo98	1.530	Fo98	7.420	Wo98	2.290	0.100	Wo98	1	Wo98	RO
						4.990	Wo98	2.440	0.090	Wo98			SA
1519-273	0.200	3.255	Fo98	0.200	Fo98	0.390	Pa99	2.030	0.430	Pa99	2	Gh93	RO
						0.320	Pa99	1.440	0.970	Pa99			SA
1532+302	0.064	0.055	NED	2.600	NED	0.760	LM99	2.000	—	LM99	1	LM99	RO
1533+342	...	0.028	NED	0.560	NED	0.400	LM99	2.600	—	LM99	1	LM99	RO
1533+535	0.890	0.030	Ba98	0.350	NED	2.390	Ba98	1.940	—	Ba98	1	Ba98	RO
1534+0148	0.312	0.034	Pa95	0.120	Pa95	0.420	Pe96	1.890	0.180	Pe96	1	Pe96	RO
1534+372	0.143	0.030	NED	0.880	NED	0.030	LM99	2.840	—	LM99	2	LM99	RO
1538+149	0.605	2.648	Fo98	0.440	Fo98	0.090	Fo98	2.050	0.900	Fo98	2	Gh93	RO
						0.280	Wo90	2.130	1.100	Wo90			EI
1541+0507	...	0.056	NED	0.120	NED	0.260	Br97	1.740	0.660	Br97	1	Br97	RO

IAU Name	z	F_R (Jy)	Ref.	F_O (mJy)	Ref.	F_X (μ Jy)	Ref.	Γ	err	Ref.	Type	Ref.	Sat
1542+614	...	0.131	NED	0.960	NED	0.120	LM99	2.500	—	LM99	2	LM99	RO
1546+027	0.413	1.450	Kh81	0.230	NED	0.840	Wo90	2.180	2.250	Wo90	3	Wo90	EI
1548+114	0.436	0.410	VV93	0.500	Gh93	0.320	Wo90	1.350	1.100	Wo90	3	Gh93	EI
1552+2020	0.222	0.038	Pa95	0.300	Pa95	1.570	Pe96	1.790	0.140	Pe96	1	Pe96	RO
1553+113	0.360	0.636	Pa95	4.800	Pa95	13.420	BSMc	2.850	0.040	BSMc	1	NED	SA
						14.860	TW	2.470	0.180	TW		AS	
						7.660	Br94	2.490	0.250	Br94		RO	
1602+308	...	0.013	Br97	0.230	NED	0.160	Br97	2.560	0.890	Br97	1	Br97	RO
1611+343	1.404	2.671	Fo98	0.350	Fo98	0.240	Fo98	1.760	0.060	Fo98	3	IT90	RO
1614+051	3.197	0.850	Ca97	0.060	Ca97	0.030	Ca97	1.600	—	Ca97	3	Ca97	AS
1626+352	0.500	0.014	LM99	0.140	LM99	0.160	LM99	1.890	—	LM99	1	LM99	RO
1631+4217	0.468	0.006	Na96	0.040	NED	0.860	Ba98	1.910	—	Ba98	1	Ba98	RO
1633+382	1.814	2.929	Fo98	0.230	Fo98	0.420	Fo98	1.530	0.080	Fo98	3	Gh93	RO
						0.250	Ku98	1.510	0.320	Ku98		AS	
1641+399	0.594	7.821	Fo98	0.890	Fo98	0.700	Wo90	1.430	0.350	Wo90	3	Gh93	EI
						0.980	Fo98	1.850	0.230	Fo98		RO	
1642+458	0.223	0.111	NED	0.350	NED	0.260	Ba98	2.360	—	Ba98	1	Ba98	RO
1652+398	0.034	1.443	Fo98	10.970	Fo98	46.420	Gh98	1.800	0.020	Gh98	1	Gh93	SA
						23.440	Ku98	2.220	0.020	Ku98		AS	
						13.400	Wo90	2.090	0.170	Wo90		EI	
						8.300	Fo98	2.630	0.050	Fo98		RO	
						12.900	Sa94	2.500	0.100	Sa94		EX	
1652+403	...	0.011	LM99	1.060	NED	0.030	LM99	2.800	—	LM99	1	LM99	RO
1704+607	0.280	0.002	VV93	0.070	NED	0.160	La96	2.360	0.350	La96	1	La96	RO
1704+716	...	0.041	NED	0.480	NED	0.160	LM99	3.100	—	LM99	1	LM99	RO
1717+178	...	0.940	Pa95	0.140	NED	0.480	Wo90	2.540	2.100	Wo90	2	Wo90	EI
1721+343	0.206	0.468	NED	0.980	NED	1.990	Wo90	1.500	0.350	Wo90	3	Wo90	EI
1722+119	0.018	0.094	Pa95	1.740	Pa95	3.600	Sa94	2.650	0.250	Sa94	1	NED	EX
1727+502	0.055	0.159	Fo98	1.700	Fo98	3.630	Fo98	2.390	0.080	Fo98	1	Gh93	RO
						3.720	Sa94	2.820	0.210	Sa94		EX	
1732+389	0.976	0.845	NED	0.110	NED	0.050	Sa97b	1.580	0.380	Sa97b	3	Sa97b	RO
1741+196	0.084	0.339	NED	0.900	NED	1.610	Sb99	2.100	0.080	Sb99	1	Br97	SA
						1.280	Br97	1.980	0.180	Br97		RO	
1742+597	...	0.089	NED	1.370	NED	0.030	LM99	2.960	—	LM99	2	LM99	RO
1746+470	1.484	0.631	NED	0.010	NED	0.020	LM99	3.080	—	LM99	2	LM99	RO
1747+433	...	0.360	NED	0.640	NED	0.050	LM99	2.320	—	LM99	2	LM99	RO
1748+470	0.160	0.010	LM99	0.110	LM99	0.540	LM99	1.940	—	LM99	1	LM99	RO
1749+096	0.322	1.973	Fo98	1.130	Fo98	0.150	Fo98	1.450	1.430	Fo98	2	Gh93	RO
						0.760	Sa97	1.890	0.080	Sa97		AS	
						0.370	Wo90	1.150	1.100	Wo90		EI	
1749+701	0.770	2.113	Fo98	0.960	Fo98	0.150	Fo98	2.440	0.710	Fo98	2	Gh93	RO
1755+552	...	0.007	Br97	0.490	NED	0.940	Br97	2.640	0.190	Br97	1	Br97	RO
1757+7034	0.407	0.007	Pa95	0.170	Pa95	0.470	Pe96	2.120	0.130	Pe96	1	Pe96	RO
1803+784	0.684	3.016	Fo98	0.610	Fo98	0.240	Pa99	1.450	0.130	Pa99	2	Gh93	SA
						0.260	Fo98	2.420	0.450	Fo98		RO	
						0.220	Wo90	1.460	1.000	Wo90		EI	
1807+698	0.051	1.713	Fo98	5.180	Fo98	0.300	Pa99	1.740	0.240	Pa99	2	Gh93	SA
						0.520	TW	1.750	0.060	TW		AS	
						0.400	Wo90	1.660	0.420	Wo90		EI	
						0.350	Co95	2.220	0.110	Co95		RO	
						2.570	Sa94	1.950	0.460	Sa94		EX	
1808+468	...	0.056	NED	0.450	NED	0.060	LM99	2.700	—	LM99	2	LM99	RO
1811+442	...	0.030	NED	0.350	NED	0.070	LM99	2.180	—	LM99	1	LM99	RO
1823+568	0.664	1.905	Fo98	0.180	Fo98	0.270	Pa99	1.960	0.350	Pa99	2	IT91	SA
						0.410	Pa99	1.150	0.190	Pa99		RO	
1829+540	...	0.024	NED	0.770	NED	0.060	LM99	3.310	—	LM99	1	LM99	RO
1838+480	...	0.032	NED	0.900	NED	0.100	LM99	3.100	—	LM99	1	LM99	RO
1841+591	0.530	0.006	LM99	0.220	NED	0.010	LM99	3.540	—	LM99	2	LM99	RO
1845+797	0.056	4.450	Kh81	8.060	NED	3.630	Sa94	1.740	0.200	Sa94	3	Gh93	EX
						5.470	Le97	1.820	0.030	Le97		AS	

IAU Name	z	F_R (Jy)	Ref.	F_O (mJy)	Ref.	F_X (μ Jy)	Ref.	Γ	err	Ref.	Type	Ref.	Sat
1848+427	...	0.007	Br97	0.200	NED	1.810	Br94	2.170	0.220	Br94	1	Br94	RO
1921-293	0.352	12.696	NED	0.840	NED	0.770	Wo90	1.570	1.300	Wo90	3	Gh93	EI
						0.380	Go95	1.670	0.270	Go95			EX
						1.060	Sa97b	1.890	0.050	Sa97b			RO
1928+738	0.360	3.339	Fo98	1.110	Fo98	0.520	Go95	2.250	0.480	Go95	3	Gh93	EX
						1.470	Fo98	2.330	0.190	Fo98			RO
1959+650	0.048	0.251	Fo98	17.490	Fo98	9.200	BSMc	2.680	0.050	BSMc	1	BSMc	SA
2005-489	0.071	1.252	Fo98	12.470	Fo98	5.400	Sa94	3.200	0.700	Sa94	1	Co97	EX
						25.380	Pa98	2.320	0.040	Pa98			SA
						5.000	Fo98	2.940	0.060	Fo98			RO
2007+777	0.342	1.364	Fo98	0.770	Fo98	0.360	Wo90	5.110	4.800	Wo90	2	Gh93	EI
						0.170	Fo98	1.750	0.560	Fo98			RO
2032+107	0.601	0.770	Pa95	1.000	Pa95	1.220	Wo90	2.430	1.400	Wo90	2	Wo90	EI
2039+523	...	0.025	NED	1.420	NED	0.230	Br97	2.800	0.890	Br97	1	Br97	RO
2126-158	3.268	1.240	Ca97	0.580	Ca97	0.720	Ca97	1.530	0.300	Ca97	3	Ca97	RO
						0.860	Ca97	1.680	0.090	Ca97			AS
						0.710	Wo90	3.180	2.100	Wo90			EI
2131-021	0.557	2.390	Fo98	0.130	Fo98	0.050	Fo98	2.050	0.460	Fo98	2	IT90	RO
2134+004	1.936	12.249	Fo98	0.720	Fo98	0.260	Fo98	1.820	0.420	Fo98	3	Gh93	RO
2136-428	...	0.108	NED	0.390	NED	0.120	La96	3.200	0.410	La96	2	La96	RO
2143+0704	0.237	0.050	Pa95	0.230	Pa95	0.120	Pe96	2.910	0.320	Pe96	1	Pe96	RO
2149-306	2.345	1.150	NED	0.710	NED	0.880	Sb96	2.040	0.940	Sb96	3	Ca97	RO
						0.760	El99	1.370	0.030	El99			SA
						1.270	Ca97	1.540	0.050	Ca97			AS
2155-152	0.672	2.150	NED	0.420	NED	0.220	Sa97b	2.170	0.100	Sa97b	3	Sa97b	RO
2155-304	0.117	0.310	Fo98	18.950	Fo98	41.050	Sa94	2.630	0.080	Sa94	1	Co97	EX
						5.980	Wo90	2.610	0.180	Wo90			EI
						44.900	Ku98	2.620	0.010	Ku98			AS
						43.900	Fo98	2.340	0.030	Fo98			RO
						73.550	Gi98	2.880	0.050	Gi98			SA
2200+420	0.069	4.857	Fo98	5.450	Fo98	2.200	Pa99	1.830	0.080	Pa99	2	Gh93	SA
						4.320	Wo90	2.340	1.900	Wo90			EI
						2.220	Sa97	1.960	0.040	Sa97			AS
						0.880	Fo98	1.920	0.470	Fo98			RO
2201+171	1.080	0.843	NED	0.120	NED	0.080	Wo90	1.410	0.800	Wo90	3	Wo90	EI
2208-137	0.392	0.580	NED	0.660	NED	0.960	Sa94	1.400	0.900	Sa94	3	Sa94	EX
2223-052	1.404	4.519	Fo98	1.020	Fo98	1.460	Wo90	1.340	0.720	Wo90	3	Gh93	EI
						0.270	Fo98	2.090	0.230	Fo98			RO
						0.220	BSGh	1.730	0.210	BSGh			SA
2230+114	1.037	3.689	Fo98	0.690	Fo98	0.420	Ku98	1.580	0.120	Ku98	3	Ku98	AS
						0.730	Tv99	1.510	0.040	Tv99			SA
						0.730	Tv99	1.510	0.040	Tv99			SA
2240-260	0.774	1.203	Fo98	0.260	Fo98	0.070	Fo98	1.790	0.400	Fo98	2	NED	RO
2243+203	...	0.120	NED	2.900	NED	0.060	LM99	2.680	—	LM99	2	LM99	RO
2247+381	0.119	0.119	NED	6.840	NED	0.600	LM99	2.510	—	LM99	1	LM99	RO
2251+158	0.859	8.759	Fo98	1.020	Fo98	1.310	Wo90	1.830	1.750	Wo90	3	IT90	EI
						1.370	Fo98	1.620	0.040	Fo98			RO
2254+024	2.090	0.426	NED	0.230	NED	0.150	Wo90	3.870	3.300	Wo90	3	Wo90	EI
2254+074	0.190	1.216	Fo98	0.600	Fo98	0.080	Wo90	0.950	2.100	Wo90	2	Gh93	EI
						0.090	Fo98	2.890	0.610	Fo98			RO
2316-423	0.055	0.540	Pa95	5.770	Pa95	0.100	Xu99	2.600	0.300	Xu99	2	Xu99	AS
						0.360	Xu99	2.000	0.200	Xu99			RO
2319+161	...	0.024	LM99	0.720	NED	0.360	LM99	2.200	—	LM99	1	LM99	RO
2322+346	0.098	0.076	NED	11.890	NED	0.420	LM99	1.800	—	LM99	1	LM99	RO
2344+514	0.044	0.215	Co97	2.370	Co97	4.170	TW	2.310	0.070	TW	1	Co97	AS
						5.180	TW	2.390	0.080	TW			AS
						5.260	TW	2.130	0.030	TW			AS
						3.400	Gi99	2.310	0.050	Gi99			SA
						6.870	Gi99	1.770	0.040	Gi99			SA
2356-309	0.165	0.029	NED	0.700	NED	5.780	Cs00	2.100	0.050	Cs00	1	NED	SA

Table 5. column (1): name of the source (IAU); (2): redshift; (3): radio flux at 5 GHz in Jy; (4): reference for the radio flux; (5): optical flux at 5500 Å; (6): reference for the optical flux; (7): X-ray flux at 1 keV in μ Jy; (8): reference for the X-ray flux; (9): X-ray photon spectral index; (10): error on the X-ray spectral index; (11): reference for the X-ray

Ba94:	Bade et al. (1994)	Gh99:	Ghisellini et al. (1999)	Pa95:	Padovani et al. (1995)
Ba98:	Bade et al. (1998)	BSGh:	Ghisellini in BeppoSAX Archive	Pa99:	Padovani et al. (1999)
Br85:	Bregman et al. (1985)	Gi98:	Giommi et al. (1998)	Pe96:	Perlman et al. (1996)
Br94:	Brinkmann et al. (1994)	Gi99:	Giommi et al. (1999)	Sa94:	Sambruna et al. (1994)
Br97:	Brinkmann et al. (1997)	Go95:	Ghosh et al. (1995)	Sa97a:	Sambruna et al. (1997)
Ca97:	Cappi et al. (1997)	Gr96:	Greiner et al. (1996)	Sa97b:	Sambruna et al. (1997)
Co95:	Comastri et al. (1995)	Kh81:	Khuer et al. (1981)	Sa99:	Sambruna et al. (1999)
Co97:	Comastri et al. (1997)	Ku98:	Kubo et al. (1998)	Sb96:	Siebert et al. (1996)
Cs00:	Costamante et al. (2000)	IT90:	Impey et al. (1990)	Sb99:	Siebert et al. (1999)
El99:	Elvis et al. (1999)	IT91:	Impey et al. (1991)	Sn97:	Sing et al. (1997)
Fa97:	Fabian et al. (1997)	La96:	Lamer et al. (1996)	Ta00:	Tagliaferri et al. (2000)
Fa98:	Fabian et al. (1998)	Le97:	Leighly et al. (1997)	Tv99:	Tavecchio et al. (2000)
Fo98:	Fossati et al. (1998)	LM99:	Laurent-Muehleisen et al. (1999)	VV93:	Veron-Cetty et al. (1993)
Fo98b:	Fossati et al. (1998)	Ma98b:	Maraschi et al. (1998)	Xu99:	Xue et al. (1999)
Ge96:	George et al. (1996)	BSMc:	Maccacaro in BeppoSAX Archive	Ya98:	Yaqoob et al. (1998)
Gh93:	Ghisellini et al. (1993)	Na96:	Nass et al. (1996)	Wa99:	Watson et al. (1999)
Gh98:	Ghisellini (1998)	NED:	NASA-IPAC Extragalactic Database	Wo98:	Wolter et al. (1998)
Gh98b:	Ghisellini et al. (1998)	Or98:	Orr et al. (1998)	Wo90:	Worrall et al. (1990)

Table 6. References used in Table 7. TW means This Work.**Fig. 17.** Optical to X-ray vs. radio to X-ray broad band indices. Circles: HBL, Squares: LBL, Triangles: FSRQs.**Fig. 18.** Radio to optical vs. radio to X-ray broad band indices. Circles: HBL, Squares: LBL, Triangles: FSRQs.

References

- Bade N., Fink H.H. & Engels D., 1994, A&A, 286, 381
 Bade N., Beckmann V., Douglas N.G. Barthel P.D., Engels D., Cordis L., Nass P. & Voges W., 1998, A&A, 334, 459
 Bregman J.N., Glassgold A.E., Huggins P.J. & Kinney A.L., 1985, ApJ, 291, 505
 Brinkmann W. & Siebert J., 1994, A&A, 285, 812
 Brinkmann W., Siebert J., Feigelson E.D. et al., 1997, A&A, 323, 739
 Cappi M., Matsuoka M., Comastri A., Brinkmann W., Elvis M., Palumbo G.G.C. & Vignali C., 1997, ApJ, 478, 492
 Comastri A., Molendi S. & Ghisellini G., 1995, MNRAS, 277, 297
 Comastri A., Fossati G., Ghisellini G. & Molendi S., 1997, ApJ, 480, 534
 Costamante L., Ghisellini G., Giommi P. et al., 2000, in "X-ray '99: Stellar Endpoints, AGN and the Diffuse Background", in press (astro-ph/0001410)
 Danly L., Lockman F. J., Meade M. R. & Savage B. D. 1992, ApJS, 81, 125
 Dickey J.M. & Lockman F.J., 1990, ARA&A, 28, 215
 Elvis M., Lockman F. J. & Wilkes B. J. 1989, AJ, 97, 777
 Elvis M., Fiore F., Siemiginowska A., Mathur S., McDowell J. & Bechtold J., 1999, HEAD, 31, 2305
 Fabian A.C., Brandt W.N., McMahon R.G. & Hook I.M., 1997, MNRAS, 291, L5
 Fabian A.C., Iwasawa K., McMahon R.G., Celotti A., Brandt W.N. & Hook I.M., 1998, MNRAS, 295, L25
 Fossati G., Celotti A., Ghisellini G. & Maraschi L., 1997, MNRAS, 289, 136
 Fossati G., Maraschi L., Celotti A., Comastri A. & Ghisellini G., 1998, MNRAS, 299, 433

- Fossati G., Chiappetti L., Celotti A. et al., 1998, Nuclear Physics B (p.s.) 69/1-3, 423
- George I.M. & Turner T.J., 1996, ApJ, 461, 198
- Ghisellini G., Padovani P., Celotti A. & Maraschi L., 1993, ApJ, 407, 65
- Ghisellini G. & Madau P., 1996, MNRAS, 280, 67
- Ghisellini G., 1998, Nuclear Physics B (p.s.) 69/1-3, 397
- Ghisellini G., Tagliaferri G., Costamante L. et al., 1998, Nuclear Physics B (p.s.) 69/1-3, 427
- Ghisellini G., Tagliaferri G. & Giommi P., 1999, IAUC 7116
- Giommi P., Padovani P. & Perlman E., 1998, Nuclear Physics B (p.s.) 69/1-3, 407
- Giommi P., Fiore F., Guainazzi M. et al., 1998, A&A, 333L, 5
- Giommi P., Massaro E., Chiappetti L. et al., 1999, A&A, 351, 59
- Ghosh K.K. & Soundararajaperumal S., 1995, ApJS, 100, 37
- Greiner J., Danner R., Bade N., Richter G.A., Kroll P., & Komossa S., 1996, A&A, 310, 384
- Kellermann K.I., Sramek R., Schmidt M., Shaffer D.B. & Green R., 1989, AJ, 98, 1195
- Kuehr H., Witzel A., Pauliny-Toth I.I.K. & Nauber U., 1981, A&AS, 45, 367
- Kubo H., Takahashi T., Madejski G., Tashiro M., Makino F., Inoue S. & Takahara F., 1998, ApJ, 504, 693
- Impey C.D. & Tapia S., 1990, ApJ, 354, 124
- Impey C.D., Lawrence C.R. & Tapia S., 1991, ApJ, 375, 46
- Lamer G., Brunner H. & Staubert R., 1996, A&A, 311, 384
- Leighly K.M., O'Brien P.T., Edelson R., George, I.M., Malkan, M.A., Matsuoka M., Mushotzky R.F. & Peterson B.M., 1997, ApJ, 483, 767
- Laurent-Muehleisen S.A., Kollgaard R.I., Ryan P.J., Feigelson E.D., Brinkmann W. & Siebert J., 1997, A&AS, 122, 235
- Laurent-Muehleisen S.A., Kollgaard R.I., Feigelson E.D., Brinkmann W. & Siebert J., 1999, ApJ, 525, 127
- Lockman F. J. & Savage B. D. 1995, ApJS, 97, 1
- Mannheim K., 1993, A&A, 269, 67
- Maraschi L., Ghisellini G. & Celotti A., 1992, ApJ, 397L, 5
- Maraschi L., Celotti A., Fossati G. et al., 1998, Nuclear Physics B (p.s.) 69/1-3, 453
- Murphy E. M., Lockman F. J., Laor A., & Elvis M. 1996, ApJS, 105, 36
- Nass P., Bade N., Kollgaard R.I., Laurent-Muehleisen S A., Reimers D. & Voges W., 1996, A&A, 309, 419
- Orr A., Yaqoob T., Parmar A.N., Piro L., White N.E. & Grandi P., 1998, A&A, 337, 685
- Padovani P. & Giommi P., 1995, MNRAS, 277, 1477
- Padovani P., Morganti R., Siebert J., Siebert J., Vagnetti F. & Cimatti A., 1999, MNRAS, 304, 829
- Perlman E.S., Stocke J.T., Wang Q.D. & Morris, S.L., 1996, ApJ, 456, 451
- Reeves J.N., Turner M.J.L., Ohashi T. & Kii T., 1997, MNRAS, 292, 468
- Sambruna R.M., Barr P., Giommi P., Maraschi L., Tagliaferri G. & Treves, A., 1994, ApJS, 95, 371
- Sambruna R.M., George I.M., Madejski G., Urry C.M., Turner T.J., Weaver K.A., Maraschi L. & Treves, A. 1997, ApJ, 483, 774
- Sambruna R.M., 1997, ApJ, 487, 536
- Sambruna R.M., Ghisellini G., Hooper E., Kollgaard R.I., Pesce J.E. & Urry C.M., et al., 1999, ApJ, 515, 140
- Sambruna R.M., Chou L.L. & Urry C.M., 2000, ApJ, 533, 650
- Siebert J., Matsuoka M., Brinkmann W., Cappi M., Mihara T. & Takahashi T., 1996, A&A, 307, 8
- Siebert J., Brinkmann W., Gliozzi M., Laurent-Muehleisen S.A. & Matsuoka M., 1999, AN, 320, 315
- Sikora M., Begelman M.C. & Rees M.J., 1994, ApJ, 421, 153
- Sing K.P., Shrader C.R. & George I.M., 1997, ApJ, 491, 515
- Tagliaferri G., Ghisellini G., Giommi P. et al., 2000, A&A, 354, 431
- Tanaka Y. et al., 1994, PASJ, 46, L37
- Tavecchio F., Maraschi L., Ghisellini G. et al., 2000, ApJ in press (astro-ph/0003019)
- Veron-Cetty M.P.; Veron P., 1993, ESO Scientific Report, Garching
- Xue S.J. & Zhang Y.H., 2000, in "X-ray '99: Stellar Endpoints, AGN and the Diffuse Background" , in press (astro-ph/9911293)
- Yaqoob T., George I.M., Turner T.J., Nandra K., Ptak A. & Serlemitsos P.J., 1998, ApJ, 505, L87
- Watson D., Hanlon L., McBreen D. et al., 1999, A&A, 345, 414
- Wolter A., Comastri A., Ghisellini G. et al., 1998, A&A, 335, 899
- Worrall D.M. & Wilkes B.J., 1990, ApJ, 360, 396